

Dynamics of advection-driven upwelling over a shelf break submarine canyon

S. E. Allen¹ and B. M. Hickey²

Received 17 August 2009; revised 30 March 2010; accepted 16 April 2010; published 19 August 2010.

[1] The response over a submarine canyon to a several day upwelling event can be separated into three phases: an initial transient response; a later, much longer, “steady” advection-driven response; and a final relaxation phase. For the advection-driven phase over realistically steep, deep, and narrow canyons with near-uniform flow and stratification at rim depth, we have derived scale estimates for four key quantities. Observations from 5 real-world canyon studies and 3 laboratory studies are used to validate the scaling and estimate the scalar constant for each scale. Based on 4 geometric parameters of the canyon, the background stratification, the Coriolis parameter, and the incoming current, we can estimate (1) the depth of upwelling in the canyon to within 15 m, (2) the deep vorticity to within 15%, and (3) the presence/absence of a rim depth eddy can be determined. Based on laboratory data, (4) the total upwelling flux can also be estimated. The scaling analysis shows the importance of a Rossby number based on the radius of curvature of isobaths at the upstream mouth of the canyon. This Rossby number determines the ability of the flow to cross the canyon isobaths and generate the pressure gradient that drives upwelling in the canyon. Other important scales are a Rossby number based on the length of the canyon which measures the ability of the flow to lift isopycnals and a Burger number based on the width of the canyon that determines the likelihood of an eddy at rim depth. Generally, long canyons with sharply turning upstream isobaths, strong incoming flow, small Coriolis parameter, and weak stratification have the strongest upwelling response.

Citation: Allen, S. E., and B. M. Hickey (2010), Dynamics of advection-driven upwelling over a shelf break submarine canyon, *J. Geophys. Res.*, 115, C08018, doi:10.1029/2009JC005731.

1. Introduction

[2] Submarine canyons are ubiquitous and steep-sided features (up to 45°) that frequently indent the continental shelf as much as 60 km [Hickey, 1995]. Off the coasts of Washington State and British Columbia typical canyons are at least 600 m deep and on the order of 5–30 km wide. These features are regions of enhanced upwelling [Freeland and Denman, 1982; Hickey, 1997; Vindeirinho, 1998] and are important for cross-shelf-break exchange including nutrient flux onto the shelf [Hickey and Banas, 2008]. They are biologically active areas with dense euphausiid and fish aggregations [Pereyra et al., 1969; Mackas et al., 1997; Allen et al., 2001] during summer upwelling favorable winds.

[3] For eastern boundaries, upwelling along the coast and within the canyons occurs as a result of pulses of equatorward currents due to local alongshore wind [Hickey, 1997] or equatorward currents generated by poleward propagating

shelf-waves [Allen et al., 2001]. During an upwelling pulse, the response over the canyon can be separated into three phases: an initial transient phase (first inertial period), a near steady advection-dominated phase and a relaxation phase (after the wind-forcing dies). The initial transient phase is reasonably well explained by linear dynamics [Allen, 1996]. In this paper a dynamical analysis of the second phase will be presented. This analysis allows results obtained by observation and numerical simulation in the relatively few canyons that have been studied to be extended to other canyons.

[4] Canyons are three dimensional features with extremely steep bottom slopes as well as sharp changes in bottom slope. Incident flow is strong and the water column can be highly stratified. Because of this challenging environment, observations within canyons sufficient to delineate the dynamics in even the most rudimentary fashion have been limited to a handful of canyons [Allen and Durrieu de Madron, 2009]. Moreover, the steep bottom slopes and strong stratification have proved to be a barrier to realistic numerical modeling studies. For example, Allen et al. [2003] have demonstrated that topography typical of many Pacific coast canyons results in numerical errors in vertical advection schemes for density. Attempts to date to model canyons using realistic topography have produced unrealistic flow and density fields where there

¹Department of Earth and Ocean Sciences, University of British Columbia, Vancouver, British Columbia, Canada.

²School of Oceanography, University of Washington, Seattle, Washington, USA.

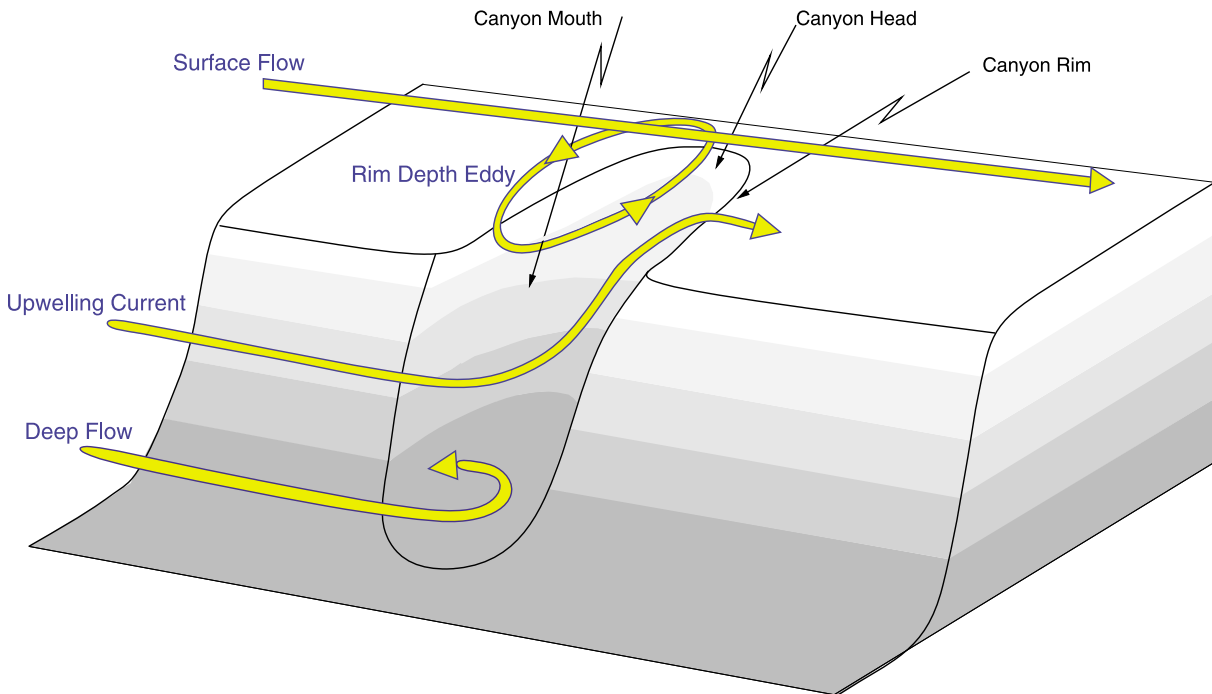


Figure 1. Schematic of the advection-driven flow over a submarine canyon.

is good observational data with which to compare [Klinck *et al.*, 1999] or have simply not had sufficient data to thoroughly test the model [e.g., Skliris *et al.*, 2001]. Even when the bottom boundary layer is well resolved, details of separation upstream of the canyon are not properly modeled [Dawe and Allen, 2010]. The goal of the present paper is to use available observations to extend the dynamical understanding obtained to the multitude of canyons that lack observations as well as to provide a dynamical framework for future modeling efforts. Such a dynamical analysis has been produced for oscillatory flow over canyons [Boyer *et al.*, 2004] although the specific length scales were not determined. Kämpf [2007] has empirically derived a scaling for upwelling flux based on numerical results.

[5] The dynamics of upwelling over a number of shelf break canyons have been examined using observations [Hickey *et al.*, 1986; Hickey, 1997; Allen *et al.*, 2001] numerical models [Klinck, 1988, 1989, 1996; Allen, 1996] and laboratory models [Allen *et al.*, 2003; Pérenne *et al.*, 2001; Mirshak and Allen, 2005]. Based on these studies the following picture of the second phase of upwelling over a canyon in a stratified environment emerges [Allen *et al.*, 2001] (Figure 1):

[6] 1. Near surface flow is only weakly affected by the canyon and passes directly over the canyon. However, near surface isopycnals may be elevated as observed over Barkley Canyon [Allen *et al.*, 2001].

[7] 2. Flow just above the depth of the canyon rim (the edge where the near flat shelf meets the steep bathymetry) flows over the upstream rim of the canyon. As it crosses the rim, it flows down into the canyon, stretching the fluid columns and generating cyclonic vorticity. The flow then turns up-canyon and flows across the canyon equatorward, shoreward and upward leaving the canyon shoreward of its

original position. As the flow crosses the canyon it decreases its depth and the stretching decreases. As the flow crosses the downstream rim, fluid columns are compressed generating anti-cyclonic vorticity. The stretching can be strong enough to generate a closed cyclonic eddy at this depth (“rim depth eddy” in Figure 1).

[8] 3. Flow over the slope at the depth of the rim of the canyon and for some depth below (“upwelling current” in Figure 1) is advected into the canyon and upwells over the downstream rim of the canyon near the head. This flow carries the deepest water advected onto the shelf. Vorticity in this flow can be generated by both flow separation [Pérenne *et al.*, 2001] and by stretching [Hickey, 1997]. Recent laboratory [Waterhouse *et al.*, 2009] and observational studies [Flexas *et al.*, 2008] suggest that the latter probably dominates.

[9] 4. The upward vertical displacement of water parcels decreases with depth. Thus water deeper than that which upwells onto the shelf is stretched within the canyon and has cyclonic vorticity (“deep flow” in Figure 1).

[10] In order for upwelling to occur within a canyon, upwelling-favorable currents must extend down to the shelf break depth. The formation of an undercurrent at shelf break depth (seasonal at Astoria Canyon) suppresses canyon upwelling [Hickey, 1997]. The results presented here are for canyons experiencing upwelling-favorable flow to shelf break depth and for canyons that behave like Barkley Canyon (located off the West Coast of Vancouver Island at latitude $48^{\circ}30'N$) and Astoria Canyon (located off the mouth of the Columbia River at latitude $46^{\circ}15'N$). In particular, the canyon must have (1) a nearly uniform flow (little horizontal shear) approaching the canyon, (2) the canyon must not approach the coast too closely, and (3) the canyon must be deep, steep and narrow. The third constraint will be made explicit during the scaling analysis. In the scaling analysis

we will assume that the cross-shelf pressure gradient is nearly uniform along the length of the canyon; this assumption requires that the approaching flow must be near uniform across the shelf over the length of the canyon. If the canyon approaches the coast closely, strong bathymetric convergences occur and their effect on the flow must be considered [Allen, 2000; Waterhouse *et al.*, 2009]. These first two provisos allow the inclusion of most canyons in the analysis. However two major west coast canyons are excluded: Monterey Bay Canyon because the regional flow is non-uniform and it cuts the continental slope all the way to the coast; and Juan de Fuca Canyon because it cuts the continental slope all the way to the coast into Juan de Fuca Strait. In our comparison to the observations we include one canyon, Redondo Canyon, which closely approaches the coast. As expected, Redondo Canyon does not follow the dynamics and scaling as well as the other canyons. For Astoria Canyon and other canyons influenced by a seasonal undercurrent at shelf break depth, observations are only considered during seasons with upwelling favorable flow extending down to shelf break depth.

2. Scaling Analysis

[11] In scale modeling of fluid flow a number of dimensionless numbers are selected that represent the essential dynamics. The laboratory parameters are then selected so that these numbers match between the real world and the laboratory. Here we will perform a scaling analysis to allow the observations from a few canyons (Astoria Canyon, Barkley Canyon, Carson Canyon, Quinault Canyon and a canyon off Tidra, North Africa) to be extended to other shelf break canyons.

[12] The dynamic parameters of the canyon upwelling problem are the incoming velocity, U , the Coriolis parameter, f , the stratification characterized by the buoyancy frequency N and the coefficient of eddy viscosity ν . We will constrain the uniformity of U and N so each is characterized by a single scale. In addition there are the geometric parameters of the system, the depth at the shelf break, H_s , the length of the canyon, L , the depth at the head of the canyon, H_h , and the width of the canyon at the shelf break W_{sb} . Three more geometric parameters define the shape of the canyon: \mathcal{R} the radius of curvature of the upstream isobaths, W the width of the canyon at mid-length and H_c the depth drop across the canyon at the shelf break. Thus we have a total of 11 parameters with two dimensions: length and time. According to the Buckingham PI theorem [Buckingham, 1914] we will have 9 non-dimensional groups.

[13] The choice of non-dimensional numbers to characterize upwelling through a canyon depends on the choice of vertical scale. For processes within the canyon the vertical scale is determined by the flow, so an obvious choice for the vertical scale is $D_H = f\ell/N$ for an appropriate horizontal length scale ℓ , which we take here as L , the length of the canyon. Given this choice for the vertical scaling, our analysis will show that the non-dimensional numbers that best characterize upwelling through a canyon are two Rossby numbers ($U/f\mathcal{R}$ and U/fL), a Burger number (NH_s/fW) and an aspect ratio (L/W_{sb}). Each Rossby number is characterized by the same velocity scale and Coriolis parameter; the length scale differs between them. Due to the three-dimensionality

of flow over canyons it is necessary to be very specific as to exactly what length scales are chosen and which parts of the flow the various numbers characterize.

[14] The other 5 non-dimensional numbers can be taken as an Ekman number: $Ek = \nu/fH_s^2$, a vertical aspect ratio, H_s/L , a measure of the slope of the continental shelf ($H_s - H_h$)/ H_s , and two additional Burger numbers $B_c = NH_c/(fW)$ and $B_s = NH_s/(fL)$.

[15] We will neglect friction, characterized by the Ekman number, Ek , in this analysis. Boundary layers will form over the shelf, in the abyss, on the slope and within the canyon. With upwelling favorable flow, these layers will have toward-coast velocities [MacCready and Rhines, 1991]. However, as the water is stratified, the Ekman layers on the slope and within the canyon will be quickly arrested [MacCready and Rhines, 1991]. In particular, considering the case of Astoria canyon, one can show that the time to complete arrest of the boundary layer between 150 and 400 m depth everywhere in the canyon is less than 1 day [Brink and Lentz, 2010; Allen and Durrieu de Madron, 2009] because slopes are larger than 0.022 (assuming a drag coefficient of 0.0029 following Brink and Lentz [2010]). Thus these boundary layers do not carry flow across isobaths and with sufficient resolution one can show they occupy only a small proportion of the volume [see Dawe and Allen, 2010, Figure 11]. Note, however, that the boundary layer on the shelf is not arrested and its impact on the shelf flow can be considerable [Jaramillo, 2005; Boyer *et al.*, 2006]. Here we take the shelf flow as a given, measured, value. Lastly, although the separation of the slope boundary layer is thought to bring vorticity into the canyon [e.g., She and Klinck, 2000], the amount of vorticity created by stretching is sufficient to account for all the vorticity measured in the field [Hickey, 1997; Allen *et al.*, 2001]. In addition, the dependence of vorticity in the canyon with stratification is consistent with stretching being the dominant mechanism in generating vorticity [Waterhouse *et al.*, 2009]. Thus, for the canyons considered here: steep-sided canyons with realistic stratification, friction is not expected to play a significant role in the dynamics within the canyon.

[16] We will assume that the flow is hydrostatic so that the vertical aspect ratio H_s/L is very small and de-couples the horizontal and vertical scales. This is a standard approximation in oceanography and has been recently verified for steep canyons [Dawe and Allen, 2010].

[17] Having eliminated the Ekman number and the vertical aspect ratio we are left with 7 non-dimensional governing parameters. The data are insufficient to allow an empirical fit to these 7 parameters. Instead we use the dynamical equations to constrain the expected response and then use the data for verification. The assumptions that the flow is hydrostatic and that friction can be neglected, along with the Boussinesq, incompressible and non-diffusive approximations are the only *a priori* assumptions we will make before writing down our starting dynamic equations. However, through the analysis we will make a number of restrictive assumptions on the flow being considered in order to simplify it. These are summarized and labeled in Section 2.5. Through this process we will find that 2 of the remaining 7 parameters play no role. The canyons under consideration will be assumed deep (Deep Canyon Assumption, see section 2.5), so that the upwelling flow does not reach the bottom of the canyon and thus the

canyon is deep enough that the total depth of the canyon H_c and its non-dimensional form B_c play no role. We will also assume that the shelf is shallow so that B_s is less than about 2 (Shallow Shelf Assumption, see section 2.5). This restriction will be explained in detail in section 2.1.1; it effectively eliminates a role for B_s .

[18] The upwelling considered in this paper is “steady” advection-driven upwelling as opposed to the transient upwelling that occurs in the initial stages of an upwelling event. The shallow water equations for steady flow of an inviscid stratified fluid are

$$\vec{u} \cdot \nabla \vec{u} - f \hat{k} \times \vec{u} = \frac{-1}{\rho_o} \nabla p \quad (1a)$$

$$\nabla \cdot \vec{u} = 0 \quad (1b)$$

$$\vec{u} \cdot \nabla \rho = 0 \quad (1c)$$

$$\frac{\partial p}{\partial z} = -\rho g \quad (1d)$$

where \vec{u} is the horizontal velocity, \hat{k} is the vertical unit vector, p is the pressure, ρ_o is a constant reference density, ρ is the density and g is the gravitational acceleration. The hydrostatic, Boussinesq, incompressible and non-diffusive approximations have been made.

[19] Taking the vertical component of the curl of equations (1a) gives a vorticity equation [e.g., *Holton, 1992*]

$$\vec{u} \cdot \nabla \zeta + (\zeta + f) \nabla_h \cdot \vec{u}_h + \nabla_h w \times \frac{\partial}{\partial z} \vec{u}_h = 0 \quad (2)$$

where \vec{u}_h , w are the horizontal components and vertical component of the velocity, respectively, ∇_h is the horizontal divergence and $\zeta = \hat{k} \cdot \nabla \times \vec{u}$ is the vertical component of the vorticity. The vorticity equation (2) consists of three terms, an advection term, a stretching term and a twisting term. The latter term corresponds to the generation of vertical vorticity by “twisting” horizontal vorticity into the vertical. As the incoming flow is usually vertically sheared (stronger near the surface), the incoming horizontal vorticity is directed onshore. However, the variations in vertical velocity occur as the flow crosses the canyon and are thus mainly directed cross-canyon. Thus the cross-product will be small and we will neglect this term. Substituting equations (1b) and equations (1c) one can derive a potential vorticity equation

$$\vec{u} \cdot \nabla \left[(f + \zeta) \left(\frac{\partial \rho}{\partial z} + \frac{\partial \rho^*}{\partial z} \right) \right] = 0 \quad (3)$$

[20] The description in the introduction illustrates that the most important characteristics of the flow within and over the canyon include: (1) the depth of upwelling; (2) the upwelling flux; (3) the presence or absence of a rim depth eddy; and (4) the vorticity of the deep flow. These characteristics are considered below in terms of similarity theory. A notation list is included for reference as needed.

2.1. Deepest Water Upwelled Onto the Shelf

[21] To determine the depth of the deepest water upwelled onto the shelf, we first estimate the strength of the flow crossing the canyon (that is, the tendency of the flow to cross the canyon rather than follow the isobaths). Then we determine the acting pressure gradient, and finally calculate the resulting deformation of the density field.

2.1.1. Tendency of the Flow to Cross the Canyon

[22] Upwelling flow through a canyon is driven by the cross-shelf pressure gradient at the depth of the rim [*Freeland and Denman, 1982; Klinck, 1989; Allen, 1996*]. The pressure field can be modified significantly by the presence of the canyon. To quantify the magnitude of the pressure gradient in the presence of the canyon consider the rim depth flow. We choose a curvilinear coordinate system that follows the shelf break isobath around the rim of the canyon. Far upstream of our (assumed isolated) canyon, the flow is rectilinear along the straight isobaths. Horizontal flow across the isobaths and vertical flow are zero. Flow along the isobaths is geostrophic and the speed is uniform. We will assume this uniform flow continues along the isobaths as it approaches the canyon and that it has a magnitude of U .

[23] The shelf break isobath at the upstream corner of the canyon is approximated as an arc of radius \mathcal{R} (Figure 2). Using polar coordinates around the projected center of this circle the vorticity ζ expands as

$$\zeta = \frac{\partial u_\theta}{\partial r} - \frac{1}{r} \frac{\partial u_r}{\partial \theta} + \frac{u_\theta}{r} \quad (4)$$

which scales as

$$\mathcal{O}(\zeta) = \frac{U}{\mathcal{R}} - \frac{V}{\mathcal{R}\pi/2} \quad (5)$$

where U is the along-isobath velocity scale, V is the cross-isobath velocity scale and $\pi/2 \approx 1$ is the approximate angle of rotation. The positive curvature (u_θ/r) has been assumed larger than the negative term $\partial u_\theta/\partial r$ because upstream the flow is uniform (Uniform Flow Assumption, see section 2.5).

[24] The potential vorticity equation (3) is essentially a balance between advection of vorticity (the first term) and stretching (the second term). Consider following a streamline from upstream, where the flow is assumed uniform, to the canyon where it crosses or follows the topography. Upstream the vorticity is zero and the density perturbation is zero so the potential vorticity is $f \partial \rho^*/\partial z$. Thus as the flow crosses the topography the vorticity will be given by

$$\zeta = f \left(\frac{\partial \rho^*/\partial z}{\partial \rho/\partial z + \partial \rho^*/\partial z} - 1 \right) \quad (6)$$

Discretizing (6) one can write

$$\zeta \approx f \left[\left(\frac{\rho_1 - \rho_b}{z_1^* - z_b^*} \right) \left(\frac{z_1 - z_b}{\rho_1 - \rho_b} \right) - 1 \right] \quad (7)$$

where we take ρ_b as the isopycnal just above the bottom boundary layer and ρ_1 as a second isopycnal at some depth above the topography where the flow is generally unaffected by the topography. The depth z_1 and z_b are the depth of ρ_1

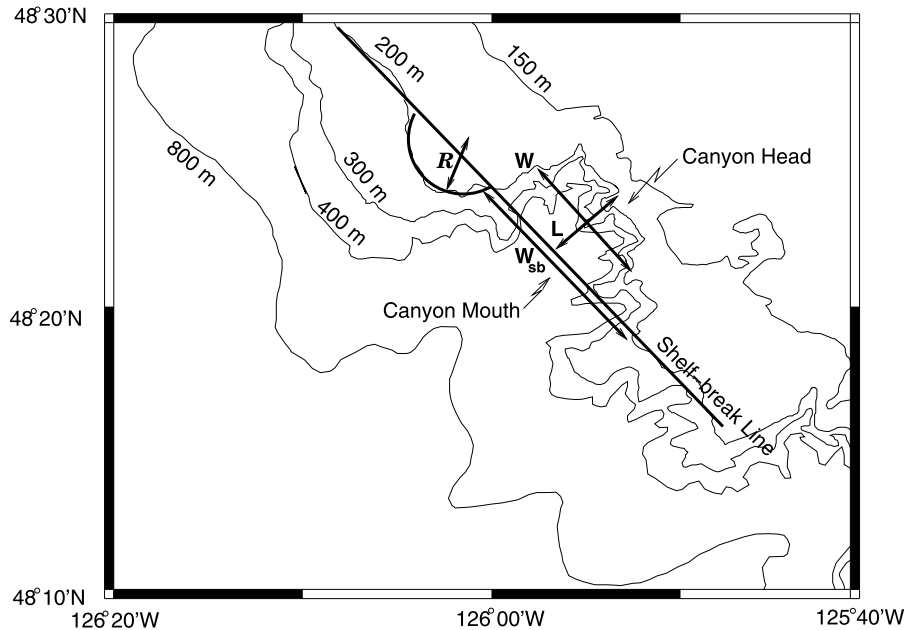


Figure 2. Plan view of the isobaths of Barkley Canyon showing the location of the shelf break, the length L , the width W , the width at the shelf break W_{sb} and the radius of curvature \mathcal{R} for this canyon as an example. One over this radius multiplied by the incoming flow and divided by the Coriolis parameter gives the Rossby number which determines the ability of the incoming flow to follow the topography.

and ρ_b , respectively and z_1'' and z_b'' are the depths of the isopycnals upstream of the canyon. If the upper isopycnal ρ_1 is far enough above the topography that it is unaffected $z_1 = z_1''$. Writing the original distance between the isopycnals as $h = z_1'' - z_b''$ and the change in depth of ρ_b as $\Delta h = z_b'' - z_b$, then (6) becomes

$$\zeta \approx f \frac{\Delta h}{h} \quad (8)$$

where we have assumed $\Delta h < h$.

[25] The change in depth Δh experienced by a column as it follows the streamline (off the lip of the canyon) is $\Delta r \partial h / \partial r$. And Δr is $v \Delta t$ and Δt is $\mathcal{R} \Delta \theta / u$ so

$$\zeta = f \frac{\Delta h}{h} = f \frac{v}{u} \frac{\mathcal{R} \Delta \theta}{h} \frac{\partial h}{\partial r} \quad (9)$$

Scaling this equation gives

$$\frac{U}{\mathcal{R}} - \frac{V}{\mathcal{R}} = f \frac{V}{U} \frac{\mathcal{R}}{h} \frac{\partial h}{\partial r} \quad (10)$$

or

$$(U - V) = \frac{V}{R_o} \quad (11)$$

where

$$R_o = \frac{U}{f \mathcal{R}} \frac{h}{\partial h / \partial r} \quad (12)$$

[26] The depth h is the vertical length scale over which isopycnals above the canyon are affected by the canyon. If the depth above the shelf break was infinite, this scale would be given by the scale depth D_h . If the depth above the shelf break is very shallow, this scale would be given by the shelf break depth H_s . The ratio of the shelf break depth to the scale depth (B_s) varies from 0.5 to 1.8 for the canyons considered here. Barkley Canyon with the 1997 stratification has the second highest value at 1.4. For this case we have clear evidence that isopycnals were affected up to the bottom of the mixed-layer at 10 m below the surface [Allen et al., 2001]. We have no detailed data for Tidra Canyon with the highest ratio. Here we will assume that the stratification is weak enough, or alternatively, the shelf break depth is shallow enough, that isopycnals are affected close to the ocean surface. This Shallow-Shelf Approximation should hold for $B_s < 1.4$ based on the Barkley Canyon observations and it may hold for higher values. Thus we take $h = H_s$.

[27] The rate of change in depth of topography $h / (\partial h / \partial r) = H_s / (\partial h / \partial r)$ is one over a length scale. We could carry this scale through our calculations but it is generally similar to the curvature \mathcal{R} . For example, the ratio of the topographic length scale to the curvature is about 0.9, 0.8, 0.7 and 1.0 for Astoria Canyon, Barkley Canyon, Carson Canyon and the laboratory canyon used by [Allen et al., 2003], respectively. Thus we assume that the change in depth of the topography scales similarly to the curvature and $R_o = U / f \mathcal{R}$ (Regular Shape Assumption, see section 2.5).

[28] A simple balance in (11) occurs for both weak incoming velocities $R_o \ll 1$ where $V \propto R_o U$ and for strong incoming velocities $R_o \gg 1$ where $V \approx U$. To exactly esti-

mate the in-between scaling for V it would be necessary to know the relative size of the coefficients in front of the terms in (11). Without this information we can write the scaling with two unknown coefficients, both expected to be of order 1. So $V = \mathcal{F}(R_o)U$ where

$$\mathcal{F}(R_o) = \frac{c_1 R_o}{c_2 + R_o} \quad (13)$$

[29] Note that if the stratification is not weak or the shelf break depth is not shallow ($B_s > 2$), $R_o = U/f\mathcal{R}$ should be replaced with $R_o = U/(f\mathcal{R}B_s) = U/(NH_s)$ (L/\mathcal{R}) which is a Froude number rather than a Rossby number.

2.1.2. Rim Depth Pressure Gradient

[30] Now that the tendency for the flow to cross the canyon has been determined, the pressure gradient along the canyon can be quantified. Returning to equations (1a) and using polar coordinates

$$u_r \frac{\partial u_\theta}{\partial r} + \frac{u_\theta}{r} \frac{\partial u_\theta}{\partial \theta} + \frac{u_\theta u_r}{r} + fu_r = \frac{-1}{\rho_o r} \frac{\partial p}{\partial \theta} \quad (14)$$

The first term is small compared to the third [see discussion below equation (5)]. By conservation of volume $1/r \partial u_\theta / \partial \theta = -\partial w / \partial z - \partial u_r / \partial r$ scales as $-V/\mathcal{R}$ and so the second two advection terms scale similarly as UV/\mathcal{R} but with opposite signs. For strong flows their sum can be shown to be zero; for weak flows they are negligible compared to the Coriolis term. Thus we neglect them and take the pressure gradient force as scaling as $fV = fU\mathcal{F}$ and the pressure gradient along the upstream rim edge of the canyon as $-\rho_o fU\mathcal{F}$. We note that here we have implicitly assumed near uniform incoming flow over the shelf for the length of the canyon (Uniform Flow Assumption, see section 2.5).

[31] The relationship between the pressure gradient and the Rossby number can be understood physically. For very wide canyons the cross-shelf pressure gradient is modified over the canyon so that the flow can smoothly follow the isobaths. A measure of the ability of the flow to follow the isobaths is given by the Rossby number ($R_o = U/f\mathcal{R}$) based on the ratio of the required acceleration of the flow to turn onshore at the upstream side of the canyon to follow the isobaths (U^2/\mathcal{R} where \mathcal{R} is the turning radius, Figure 2) to the Coriolis force fU .

[32] If the flow passes directly across the canyon (large R_o), the along-canyon pressure gradient is identical to that upstream of the canyon which, assuming geostrophy, is $\rho_o fU$. The actual pressure gradient along the canyon at the rim level is expected to be $\mathcal{O}[\rho_o fU\mathcal{F}(R_o)]$ where \mathcal{F} is an appropriate function (as derived above). Physically one can argue that for very small Rossby numbers, the flow will follow the isobaths and the pressure gradient along the canyon will be negligible (\mathcal{F} small). For very large Rossby numbers the flow will cross directly over the canyon and the pressure gradient is expected to be close to $\rho_o fU$ (\mathcal{F} order 1).

[33] The pressure difference between the canyon mouth where the canyon opens to the deep ocean (Figure 2) and the canyon head where the canyon ends on the shelf (Figure 2) is the pressure gradient multiplied by an appropriate length. Because advection onto the shelf occurs at depths near rim depth, the length L of the canyon is taken as the length from

the shelf break (canyon mouth) to the last isobath that is significantly deflected by the canyon (the canyon head).

2.1.3. Deformation of the Density Field

[34] To determine the deformation of the density field we use the natural coordinate system [e.g., Holton, 1992] where s is along the horizontal direction of the flow and n is across it. Note that this choice implies that the flow in the direction n is zero. The equations (1) become

$$u \frac{\partial u}{\partial s} = \frac{-1}{\rho_o} \frac{\partial p}{\partial s} \quad (15a)$$

$$\frac{u^2}{R} + fu = \frac{-1}{\rho_o} \frac{\partial p}{\partial n} \quad (15b)$$

$$\frac{\partial u}{\partial s} + \frac{\partial w}{\partial z} = 0 \quad (15c)$$

$$u \frac{\partial \rho}{\partial s} + w \frac{\partial \rho}{\partial z} = 0 \quad (15d)$$

$$\frac{\partial p}{\partial z} = -\rho g \quad (15e)$$

where R is the radius of curvature of the streamlines. By convention, R is taken to be positive when the curvature is to the left of the flow.

[35] Consider the deepest streamline which crosses the rim of the canyon. It comes from a depth $H_h + Z$ at the mouth of the canyon and rises a distance Z to reach the depth of the head of the canyon H_h . Along this streamline density is conserved (15d). Equation (15d) scales as

$$\frac{U_* \Gamma}{L} - \frac{\Omega \rho_o N^2}{g} = 0 \quad (16)$$

because the dominant vertical gradient of density is the undisturbed gradient $\partial \rho_o / \partial z$. The Brunt-Väisälä frequency is N where ($N^2 = -g/\rho_o \partial \rho_o / \partial z$), Γ is the scale of horizontal density perturbations, L is the length scale of the streamline, U_* is the scale of the horizontal velocity of the upwelling stream and Ω is the vertical velocity scale.

[36] By conservation of mass (15c) the horizontal and vertical velocity and linear scales are related according to

$$\frac{U_*}{L} - \frac{\Omega}{Z} = 0 \quad (17)$$

[37] This streamline marks the depth where the total pressure gradient is zero. The pressure change along the canyon that drives upwelling was estimated above as $\rho_o fUFL$ and this must balance the density gradient due to the perturbation density. Scaling (15e) gives

$$\frac{\rho_o fUFL}{Z} = \Gamma g \quad (18)$$

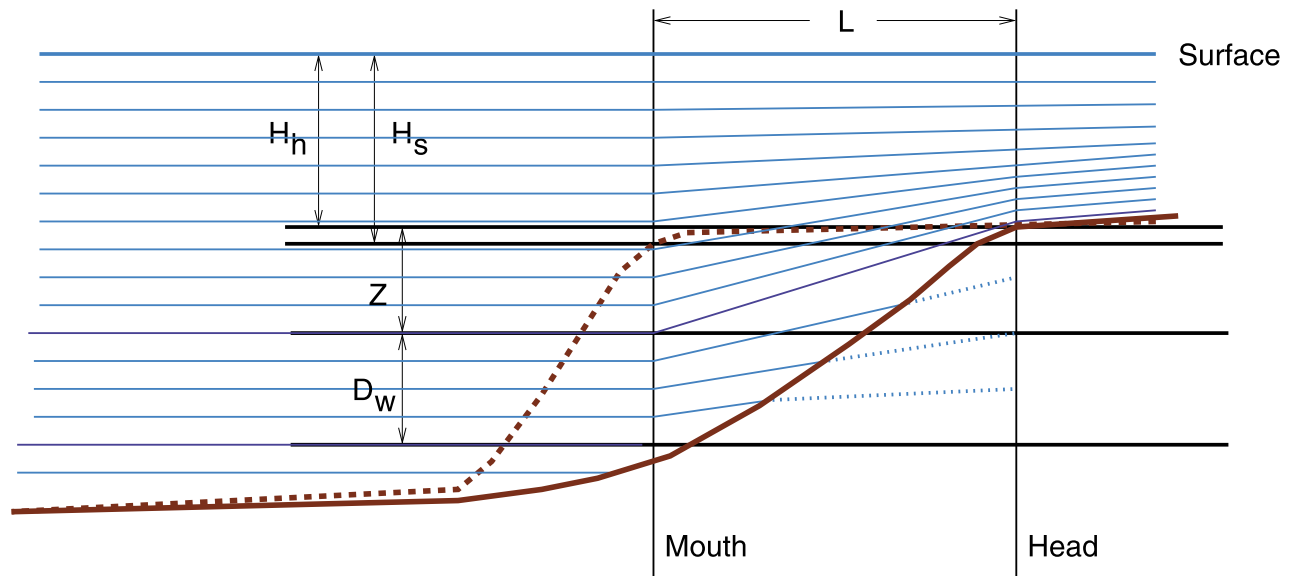


Figure 3. Sketch to illustrate the baroclinic pressure gradient due to isopycnals (thin lines) tilting towards the head of the canyon. The sketch shows a cross-section through the centreline of the canyon. The bottom-topography away from the canyon is given by the bold dashed line. The height Z is determined by balancing the pressure gradient at rim depth and the change in baroclinic pressure gradient due to the tilted isopycnals. The depth $H_h + Z$ is the deepest water upwelled onto the shelf. The column-stretching deep in the canyon is given by the ratio Z/D_w where D_w is the vertical scale within the canyon.

[38] Combining (16), (17) and (18) allows us to solve for the three scales

$$Z = \left(\frac{fUL\mathcal{F}}{N^2} \right)^{1/2} = D_H(\mathcal{F}R_L)^{1/2} \quad (19)$$

$$\Omega = U_* \left(\frac{fU\mathcal{F}}{N^2L} \right)^{1/2} = \frac{U_*D_H}{L}(\mathcal{F}R_L)^{1/2} \quad (20)$$

$$\Gamma = \left(\frac{\rho_o^2 fU\mathcal{F}N^2L}{g^2} \right)^{1/2} = \left(\frac{\partial\rho_*}{\partial z} D_H \right) (\mathcal{F}R_L)^{1/2} \quad (21)$$

where $D_H = fL/N$ and $R_L = U/(fL)$. The scale Z is the depth of upwelling, a quantity that will be compared with observations in the subsequent section. Note that here we have implicitly assumed a near uniform N value over a depth range Z below the depth of the head of the canyon (Uniform Stratification at Rim Depth Approximation, see section 2.5).

[39] One can also derive the scale for Z from physical arguments. Consider the water which passes through the mouth of the canyon and is upwelled onto the shelf. The deepest isopycnal that is upwelled onto the shelf is that one which just touches the rim of the canyon at the canyon head (depth H_h). At the canyon mouth, this isopycnal has depth $Z + H_h$. At this depth there must be a balance in the canyon such that the pressure at the mouth of the canyon is the same as that at the head (Figure 3). The tilted isopycnals provide a baroclinic pressure gradient to balance the rim depth pressure gradient so that below this isopycnal the flow does not go from the canyon up onto the shelf.

[40] Assuming that the average tilt of the isopycnals is $T = Z/L$, the density difference along the canyon (length L) is $\partial\rho_*/\partial z TL$. Thus the baroclinic pressure difference along the canyon due to the tilted isopycnals (integrating over the depth Z) is $\mathcal{O}(\rho_o N^2 Z^2)$. Equating this baroclinic pressure change and the pressure change at rim depth ($fU\rho_o L\mathcal{F}$) gives equation (19).

2.2. Upwelling Flux

2.2.1. Speed of the Upwelling Stream

[41] Quantitatively, to determine the upwelling flux through the canyon, we scale (15b). This flow lies directly below the shelf-depth flow crossing the canyon and it twists more up-canyon as it goes deeper. However, most of the upwelling stream crosses the downstream canyon rim with only a little flowing out the head of the canyon. The top of this flow is thus exposed to the same pressure gradient along-canyon as the shelf-depth flow, and the lowest part of this flow is at Z and there is no pressure gradient. Thus the flow speed varies with depth but mid-way through it will be driven by a pressure gradient 1/2 the strength of the shelf break pressure gradient immediately above the upwelling stream which is $fU\mathcal{F}$ so

$$\frac{U_*^2}{W_{sb}} + fU_* = \frac{1}{2}fU\mathcal{F} \quad (22)$$

where W_{sb} is the width of the canyon and the required turning radius for flow into the canyon. Writing $R_w = U/(fW_{sb})$ we see that for small $\mathcal{F}R_w/2$ the balance is between the last two terms. One would expect that the coefficients c_1 and c_2 in \mathcal{F} would be of order 1 which will be verified later using the data. If we assume c_1 and c_2 are 1, for all canyons

Table 1. Scales for Three Shelf Break Canyons on the West Coast of Canada and the United States, One on the East Coast of Newfoundland, One on the Northwest Coast of Africa, and Three Model Canyons Used in Laboratory Studies^a

Number	Astoria	Barkley	Quinault	Carson	Tidra	Lab-Allen	Perenne	Mirshak	Redondo
H_s	150 m	200 m	180 m	125 m	130 m	2.2 cm	2.5 cm	2.2 cm	80 m
H_h	110 m	170 m	130 m	110 m	100 m	1. cm	2.5 cm	1.0 cm	40 m
H_c	450 m	350 m	1200 m	375 m	470 m	3. cm	4. cm	3. cm	375 m
U	0.20 ms ⁻¹	0.1 ms ⁻¹	0.2 ms ⁻¹	0.1 ms ⁻¹	0.15 ms ⁻¹	1.2 cm s ⁻¹	0.8 cm s ⁻¹	0.4–1.7 cm s ⁻¹	0.15 m s ⁻¹
f	1.05×10^{-4} s ⁻¹	1.08×10^{-4} s ⁻¹	1.07×10^{-4} s ⁻¹	1.03×10^{-4} s ⁻¹	0.49×10^{-4} s ⁻¹	0.52 s ⁻¹	0.5 s ⁻¹	0.4–0.7 s ⁻¹	0.81×10^{-4} s ⁻¹
L	21.8 km	6.4 km	16.6 km	16.5 km	5.1 km	8 cm	15 cm	8 cm	8.5 km
W	8.9 km	8.3 km	30.0 km	11.8 km	10.2 km	2.4 cm	8.6 cm	2.4 cm	7.0 km
\mathcal{R}	4.5 km	5.0 km	44.0 km	18.4 km	2.7 km	1.4 cm	3.1 cm	4.0 cm	6.0 km
N	7.5×10^{-3} s ⁻¹	5.0×10^{-3} s ⁻¹ ('97) 4.5×10^{-3} s ⁻¹ ('98)	7.5×10^{-3} s ⁻¹	9.7×10^{-3} s ⁻¹	3.5×10^{-3} s ⁻¹	2.2 s ⁻¹	2.4 s ⁻¹	2.2–4.4 s ⁻¹	9.5×10^{-3} s ⁻¹
W_{sb}	15.7 km	13 km	50 km	33.7 km	8.5 km	6.9 cm	20 cm	5.8 cm	8.5 km
D_{Ht}	305 m	138 m ('97) 154 m ('98)	237 m	175 m	71 m	1.9 cm	3.1 cm	1–2.5 cm	72 m
D_W	103 m	140 m ('97') 156 m ('98)	334 m	174 m	52 m	0.8 cm	2.1 cm	0.3–0.9 cm	34 m

^aA ninth shelf break canyon, which closely approaches the coast, Redondo Canyon, is included for contrast.

for which we have found data (Table 1), \mathcal{FR}_w is less than 0.2 and so we will neglect this term (Weak to Moderate Flow Assumption, see section 2.5). Thus the upwelling stream velocity scales as UF with a coefficient expected in the range of 1/2.

[42] Physically, the upwelling stream velocity is proportional to the strength of the pressure gradient along the canyon.

[43] At this point it is useful to also consider the flow above the rim of the canyon as in practice it is difficult to distinguish these two flows. In Section 2.1.1 we separated the shelf break depth flow into two components: U , the flow following the isobaths and V , the flow crossing the isobaths. This latter flow is proportional to FU and will tend to shift shoreward as it crosses the canyon.

[44] The first component U which follows the isobaths should return to its nominal depth on the downstream side of the canyon and thus should not contribute to the upwelling flux. However, if the shelf is flat there are no topographic gradients to drive this nearly geostrophic flow back toward the shelf break. One can contrast the flow over a sloping-shelf which has a strong off-shore flow downstream of the canyon [She and Klinck, 2000, Figure 6] to the flow over a flat shelf with flow from the canyon reaching the coast [Klinck, 1996, Figure 4a; Kämpf, 2007, Figure 5]. Thus for a flat shelf this component forms part of the shoreward flux whereas for a sloped shelf it does not.

[45] We will assume the shelf is sloped. A measure of the strength of the slope is $(H_s - H_h)/H_s$ and this should be substantial compared to the strength of the geostrophic flow on the shelf, given by say $R_L = U/fL$. It is difficult to put limits on this ratio $M = (H_s - H_h)/L(H_s U)$ because observational data does not generally include the full velocity field. Our lowest non-zero value is over Tidra Canyon where $M = 0.4$. The path of a single drifter above head-depth shows flow directly along the canyon axis to the 50 m isobath [Shaffer, 1976, Figure 44] which would suggest that this might be a flat-shelf case. However, density sections up the canyon and onto the shelf [Shaffer, 1976, Figure 20] are far more similar to the sloping case [e.g., Dawe and Allen, 2010, Figure 9] than they are to the flat-bottom case [e.g., Pérenne et al., 2001, Figure 15]. The second lowest non-

zero M value is 1.1 over Barkley Canyon. Here the observations of salinity contours on a density surface show flow turning downstream at about head-depth [Allen et al., 2001]. Thus our estimate is that a critical value for M is below 1 but might indeed be below 0.4 (Sloped-shelf Approximation, see Section 2.5).

2.2.2. Upwelling Flux

[46] The flux up the canyon is the flux through the canyon mouth. The flow velocity scales as U^* and the width is W_{sb} unless the canyon width is considerably wider than the Rossby radius (Narrow Canyon Assumption, see section 2.5). The deepest water upwelled is $H_h + Z$. To calculate the upwelling flux the vertical thickness of the upwelled stream must also be estimated.

[47] At the upstream canyon rim, water from the shelf (the rim depth flow) crosses the isobaths. It drops down into the canyon and then separates from the topography. Below this flow, the upwelling stream flows nearly parallel to the isobaths as it has no shelf source. This flow is geostrophic to first order and so the pressure gradient along this line is zero. This requires a balance between the baroclinic pressure gradient due to the tilted isopycnals within the canyon and the rim depth pressure gradient. As calculated above, at the mouth, the depth at which this balance occurs is $Z + H_h$. Below this depth the water re-circulates within the canyon. But this depth is also the depth of the bottom of the rim depth flow crossing the canyon. Thus, against the upstream rim of the canyon, the depth of the top of the upwelling stream and the depth of the bottom of the upwelling stream are the same (Figure 4). Thus on the upstream side of the canyon the upwelling stream is pinched to zero vertical height [see Hickey, 1997, Figure 3].

[48] The rim depth flow crosses the canyon at an angle, is advected slightly up-canyon and crosses the downstream rim. So at the downstream rim of the canyon, the bottom of the rim depth flow is rim depth. As the top of the upwelling stream is the bottom of the rim depth flow, at the downstream rim, the top of the upwelling stream is rim depth. At the mouth of the canyon, the bottom of the upwelling stream is the depth of the deepest water upwelled, $Z + H_h$. Thus the upwelling stream forms a wedge with vertical thickness Z at the downstream side and zero vertical thickness on the

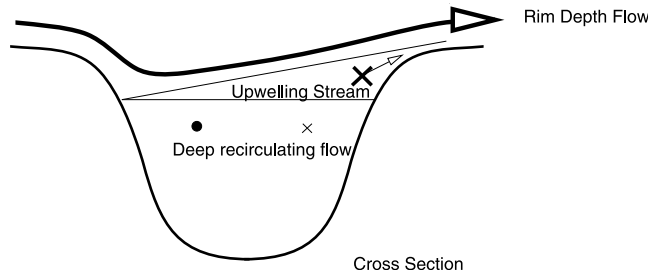


Figure 4. Cross-section through a canyon. The flow pattern is separated into three regions in the vertical: rim depth flow crossing the canyon, the upwelling stream flowing up-canyon, and the deep flow recirculating within the canyon. The upwelling stream has a strong component into the page and a weaker component across the canyon and up onto the shelf.

upstream side of the canyon. Hence for canyons narrower than the Rossby radius, the upwelling flux scales as

$$\Phi = U_* W_{sb} Z = (U W_{sb} D_H) \mathcal{F}^{3/2} R_L^{1/2} \quad (23)$$

with an expected coefficient on the order of 1/4.

2.3. Eddy Presence at Rim Depth

[49] An eddy is generated at the depth of a canyon rim due to stretching of the water column as it crosses the canyon [Hickey, 1997; Allen *et al.*, 2001]. The rim depth flow crosses the upstream canyon edge, feels the slope of the canyon, and drops down to a depth Z . The thickness of this flow is the full depth of the water column H_s , because D_H is generally larger than the depth of the water column. The stretching of this flow across the canyon is given by Z/H_s , which generates a vorticity fZ/H_s assuming conservation of potential vorticity.

[50] This cyclonic vorticity has a width given by the half-width of the canyon $W/2$ and is embedded in a flow of strength U . If the flow velocity generated by the vorticity is equal to the background flow then the total flow will be zero in one region. If the vorticity is stronger, closed streamlines will form. The circulation $2\pi uR$ around a circle of radius R due to a patch of vorticity is equal to the area of the circle multiplied by the vorticity. Thus the velocity due to the vorticity scales as fZW/H_s and an eddy forms if this velocity is large compared to the background velocity U ; that is, if

$$E = \frac{fW}{U} \frac{Z}{H_s} = \frac{1}{B_u} \left(\frac{\mathcal{F}}{R_L} \right)^{1/2} \quad (24)$$

is large, where $B_u = NH_s/fW$ and the coefficient is expected to be about 1/2.

2.4. Deep Water Vorticity

[51] Assuming conservation of potential vorticity, the stretching S of the water column multiplied by the Coriolis frequency gives the deep cyclonic vorticity. The fluid of interest is that below Z to the deepest isopycnal that is significantly elevated within the canyon. If this isopycnal occurs at scale depth D_w below Z at the mouth of the can-

yon, then the water column that has a length D_w at the mouth of the canyon has a length $Z + D_w$ near the head of the canyon (Figure 3) and $S = Z/D_w$. For a geostrophically balanced flow we would expect a vertical scale depth given by $f\ell/N$ where ℓ is an appropriate horizontal length scale. We observe that the velocity in the deep canyon is into the canyon on the downstream side and out of the canyon on the upstream side.

2.4.1. Scale Depth Deep in the Canyon

[52] To quantify the scale depth D_w , we will scale the equations for the deep cyclonic circulation. Deeper than $(Z + H_s)$, that is under the deepest isopycnal that upwells through the canyon, the pressure along the centre axis of the canyon is lower than at the side of the canyon, assuming the pressure gradient is in balance with the cyclonic circulation at depth.

[53] From (15b) and (15e) we can form the thermal wind equation

$$f \frac{\partial u}{\partial z} = \frac{g}{\rho_0} \frac{\partial \rho}{\partial n} \quad (25)$$

where we have assumed U_D/fW_{sb} is small and U_D is the velocity scale at this depth.

[54] From conservation of potential vorticity

$$\left(f + \frac{u}{R} - \frac{\partial u}{\partial n} \right) \frac{\partial \rho}{\partial z} = f \frac{\partial \rho^*}{\partial z} \quad (26)$$

and so assuming $\partial \rho / \partial z \approx \partial \rho^* / \partial z$ to first order then

$$\frac{\partial u}{\partial n} - \frac{u}{R} = f \left(\frac{\partial \rho}{\partial z} - \frac{\partial \rho^*}{\partial z} \right) \left(\frac{\partial \rho^*}{\partial z} \right)^{-1} \quad (27)$$

Combining these equations gives

$$\frac{\partial}{\partial n} \left(\frac{\partial u}{\partial n} - \frac{u}{R} \right) = \frac{f^2}{N^2} \frac{\partial^2 u}{\partial z^2} \quad (28)$$

The two terms on the left-hand side have the same sign. This flow is the deep flow in/out on the downstream/upstream side of the canyon so the cross-flow length scale is about half W_{sb} . Scaling (28) we get that vertical length scale of this flow is $D_w = fW_{sb}/2N$.

2.4.2. Deep Water Stretching

[55] The deep stretching is of order

$$S = \frac{NZ}{fW_{sb}} = (\mathcal{F}(R_o)R_L)^{1/2} \frac{L}{W_{sb}} \quad (29)$$

where the coefficient is expected to be of order 2. The vorticity deep in the canyon is given therefore by a combination of two Rossby numbers and an aspect ratio and is independent of the stratification. This independence occurs because both the drop into the canyon Z and the scale depth within the canyon D_w decrease with stratification. As stretching is a ratio between these depths, the vorticity is independent of N . Note that for canyons deeper than the depth of upwelling plus the scale depth ($D_w + Z < H_c$), the total canyon depth is unimportant because the flow does not feel the canyon bottom (Deep Canyon Assumption, see section 2.5).

Table 2. Dimensionless Parameters for Six Shelf Break Canyons and Three Laboratory Model Canyons^a

Number	Astoria	Barkley	Quinault	Carson	Tidra	Lab-Allen	Perenne	Mirshak	Redondo
R_o	0.42	0.19	0.04	0.05	1.1	1.6	0.52	0.22–0.93	0.31
\mathcal{F}	0.32	0.17	0.05	0.06	0.56	0.65	0.36	0.20–0.51	0.26
R_L	0.09	0.14	0.11	0.06	0.60	0.29	0.11	0.11–0.47	0.22
R_w	0.12	0.07	0.04	0.03	0.36	0.33	0.08	0.15–0.64	0.22
B_u	1.2	1.1 ('97) 1.0 ('98)	0.42	1.0	0.91	3.9	0.72	2.9–7.6	1.3

^aA ninth shelf break canyon, Redondo Canyon, which closely approaches the coast, is included for contrast.

2.5. Restrictions on Cases Considered

[56] During the scaling derived above we have made a number of implicit and explicit assumptions that restrict the canyons and flow under consideration. These assumptions are summarized below:

2.5.1. Uniform Flow

[57] We have assumed the incoming flow is nearly uniform along the length of the canyon and from the depth of the head of the canyon to the depth of the shelf break. As mentioned in the introduction, this eliminates a number of real world canyons.

2.5.2. Weak to Moderate Flow

[58] We have assumed that $\mathcal{F}R_w$, which is approximately a Rossby number squared, is small (<0.2). Larger flow speed would require high order terms in the upwelling flux calculation.

2.5.3. Uniform Stratification Near Rim Depth

[59] Over a scale Z the stratification $\partial\rho^*/\partial z$ or N has been assumed nearly uniform. If the value of N was 20% lower at a depth Z we would expect an under-estimate of the upwelling depth by about 10% as the back-pressure provided by the baroclinic pressure gradient would be best estimated with the average N over the depth Z rather than the value at the depth of the shelf break. An error of 10% for these scaling estimates is reasonable based on the order of the scatter in our empirical fits to observations. This constraint is met by most canyons as typically the pycnocline is much shallower than shelf break depth. For Barkley Canyon the variation in N is about 12%, for Astoria it is larger at 18% mainly due to the larger value of Z .

2.5.4. Shallow Shelf Break Depth

[60] We have assumed that the isopycnals over the canyon are affected to near the surface of the ocean so that the effective depth over the canyon is set by the shelf break depth. This assumes that B_s is not too large (<2).

2.5.5. Sloped Continental Shelf

[61] We have assumed that the continental shelf is sloped so that onshore flow is inhibited on the shelf due to its slope. This assumes that M is large: greater than 1 is a conservative limit. If the continental shelf is flat or only weakly sloped, our analysis will under-estimate the total flux onshore as it will not include a branch of the incoming flow that follows the canyon rim to the head of the canyon and is not turned back to the shelf break by the shelf-topographic slope.

2.5.6. Steep Canyon Walls

[62] We have assumed friction is not important as the bottom boundary layer will have arrested within the canyon and over the continental slope. For a given canyon, this constraint can be evaluated using the *Brink and Lentz* [2010] criteria.

2.5.7. Deep Canyon

[63] For the upwelling flux scaling we have assumed the depth of the canyon is much greater than Z . For the deep vorticity scaling we have made the stronger assumption that the scale depth, D_w is of order of, or smaller than, the depth of the canyon.

2.5.8. Narrow Canyon

[64] We have assumed, in the upwelling flux scaling, that the canyon width is narrower than about 2 Rossby radii, a . For wider canyons, $2a$ should replace W_{sb} as the width scale for the flux.

2.5.9. Regular Shape at Upstream Corner

[65] We have assumed that the topographic length scale near the upstream corner of the canyon, $H_s(\partial h/\partial r)^{-1}$, is similar to the radius of curvature of the isobaths, \mathcal{R} . This ratio is very close to one for all the canyons considered here but may eliminate certain types of canyons.

3. Scaling Applications

[66] In the following sections, the scaling analysis is applied to eight different canyons, five real world and three laboratory models. For each canyon, the maximum depth of upwelling, presence of a rim depth eddy and the deep canyon vorticity are estimated from available data. Results are compared with estimates derived from the scaling arguments and the fit between the observed and scaled results is used to estimate the scalar coefficients for the scaling factors for upwelling depth, eddy presence and deep vorticity. For contrast we also give results for Redondo Canyon which closely approaches coast and therefore can be expected to have somewhat different dynamics [Allen, 2000]. We use the information from the flux estimates of a single laboratory canyon study to compare with upwelling flux [Mirshak and Allen, 2005]. Geometric and flow characteristics for each canyon are given in Table 1. Geometric parameters are derived from bathymetric maps; flow velocity is for near rim depth and is estimated from nearby current meters; and the Brunt-Väisälä frequency is also for near rim depth and is estimated from nearby CTD casts. Non-dimensional numbers for the nine canyons are given in Table 2.

[67] Four of the canyons are located on the U.S. or Canadian west coast. One canyon is on the northwest coast of Africa and one is on the east coast of Newfoundland. The first five are subject to intermittent upwelling conditions whereas Carson Canyon off the coast of Newfoundland only occasionally receives upwelling-favorable flow. The shelf width varies from about 30 km to 60 km. Redondo Canyon extends closest to the coast (2 km). Widths vary from about 8 km (Barkley) to 30 km (Quinault). A variety of shapes are

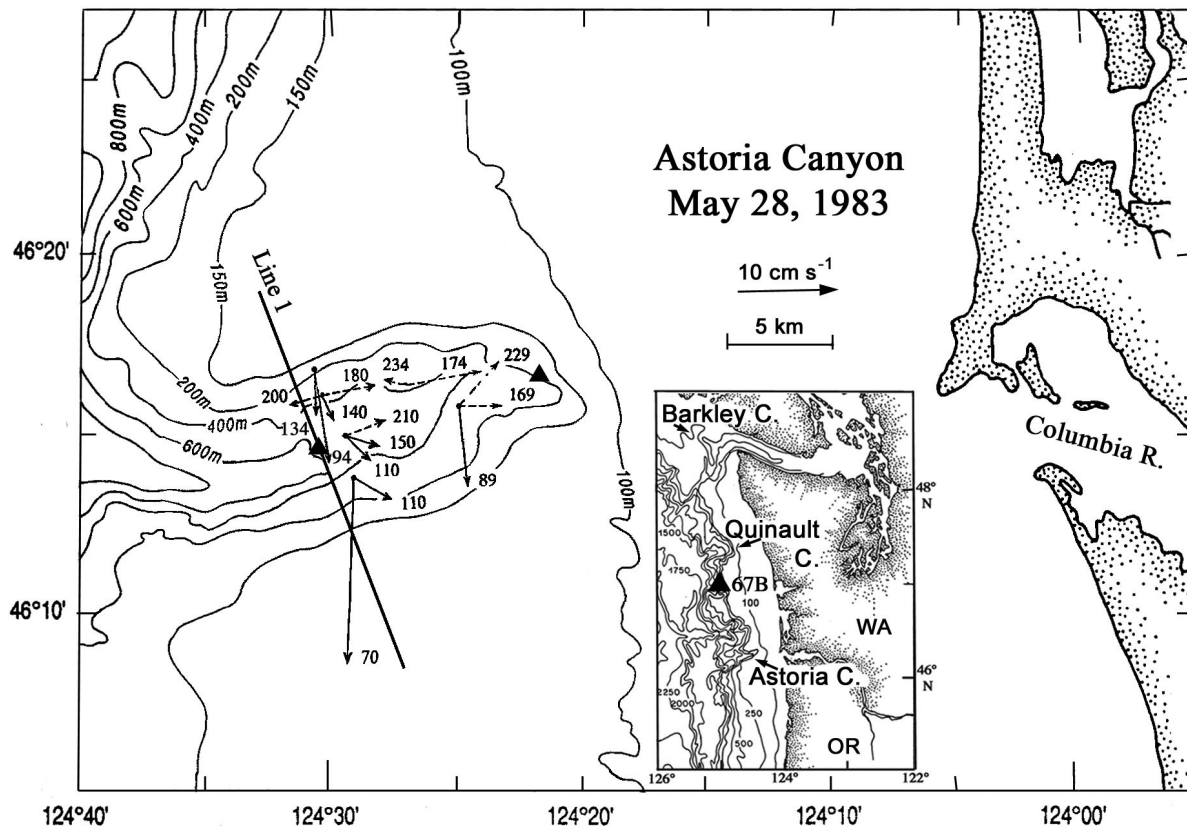


Figure 5. Bathymetry of Astoria Canyon. Inset shows the locations of Astoria Canyon, Barkley Canyon, and Quinault Canyon. Mean currents above and below the rim are shown as solid and dotted arrows, respectively. Note the tendency for the near-surface flow above 100 m to pass unaffected over the canyon, the rim depth (150-m) flow to go up the canyon and the deep flow to form a possibly closed cyclonic gyre. The two CTD stations used for estimating the depth of upwelling are marked with triangles. The solid straight line marks a detailed hydrographic survey line along which stretching was calculated.

represented, from the squat Barkley canyon to a long, thin laboratory canyon.

3.1. Available Data

[68] Astoria canyon is a narrow, deep canyon (9 km by 600 m) situated off the U.S. west coast just offshore of the Columbia River (Figure 5). The walls of Astoria canyon are steep, approaching 45° in some locations. The canyon is relatively symmetrical in shape and is aligned such that the canyon axis is roughly perpendicular to the direction of the local isobaths. Since the shelf circulation is quasi-geostrophic, the regional flow follows the northwest to southeast direction of the local isobaths to intersect the canyon axis at roughly right angles [Hickey, 1989]. An 18 element moored velocity/temperature array deployed for several months during the early upwelling season as well as CTD/transmissometer surveys during one strong upwelling event have been used to provide valuable “ground truth” data for model studies of submarine canyons [e.g., Klinck *et al.*, 1999]. The data used in this study were all obtained prior to the development of a poleward undercurrent at the shelf break depth [Hickey, 1997]. The data has proved especially valuable because moorings were placed at closely spaced ($\approx 2\text{--}5$ km) intervals both along and across the canyon (Figure 5). The data were used to provide time- and space-dependent estimates of

vertical velocity and of relative and stretching vorticity. These estimates were compared with results from available models as well as with along-shelf wind and velocity incident on the canyon to provide a detailed description of time variable upwelling within a canyon [Hickey, 1997].

[69] Barkley Canyon is situated off the southern end of Vancouver Island (Figure 5). The shelf in this region is wide (60 km) and shelf break depth deep (200 m). In this region, shelf waves propagating from the south can have a stronger effect on long-shore currents than the local wind [Hickey *et al.*, 1991]. The California Undercurrent is somewhat deeper (core at 400–500 m depth) off Vancouver Island than it is further south and it does not penetrate onto the shelf near Barkley Canyon [Krassovski, 2008]. Barkley Canyon is short (17 km) for its width (8 km) (Figure 6). Incident flow is approximately perpendicular to the canyon axis. In 1997 four current meter moorings were deployed in the canyon (Figure 6) and a detailed CTD survey of the region was performed [Vindeirinho, 1998; Allen *et al.*, 2001]. The CTD survey extended both upstream and downstream from the canyon which allowed the use of diagnostic model to determine the mean currents around the canyon [Allen *et al.*, 2001]. These currents clearly show a strong, closed eddy at rim depth (Figure 6). The study was repeated in 1998. Conditions differed from 1997; a summer storm of maxi-

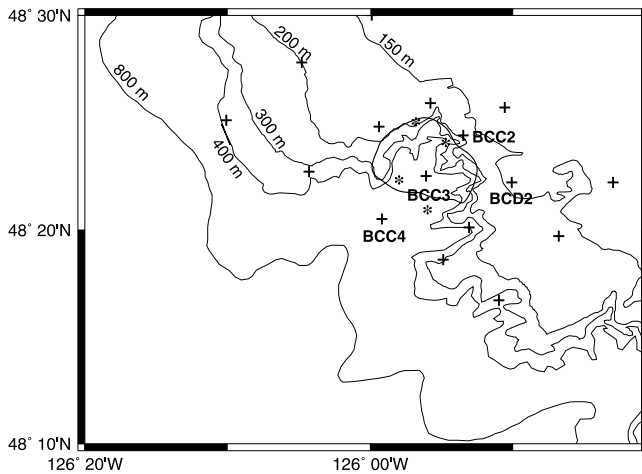


Figure 6. CTD stations (pluses) and moorings (asterisks) around Barkley Canyon in July 1997. The thick solid line is a closed streamline at 150 m depth from a diagnostic model inversion of the density field. This streamline shows the boundary of a closed eddy about 50-m above rim depth (200-m). The moorings were in the same position in 1998.

mum wind speed 14 m s^{-1} on Jul 14 reversed upwelling currents from Jul 11–21, several days before the CTD survey over the canyon which was completed on Jul 25. The lack of a synoptic CTD survey meant the diagnostic model could not be used for 1998.

[70] Quinault submarine canyon is a broad, relatively deep canyon ($\approx 30 \text{ km}$ by 1200 m) located off the Washington coast 60 km north of Astoria canyon (Figure 7). Quinault is subject to roughly the same environmental conditions as Astoria canyon because both wind stress and ambient currents are large scale in this region [Hickey, 1989]. Quinault Canyon was studied with current meters and sediment traps primarily placed along the axis and with CTD surveys along and across the canyon [Hickey, 1989].

[71] A scaled physical model of a shelf/slope geometry including a canyon in a stratified density field was constructed in the laboratory (Figure 8) [Allen *et al.*, 2003]. The Lab-Allen canyon shelf break depth is 2.2 cm and the depth at the head of the canyon is 1 cm. The canyon is 7 cm wide, 8 cm long and strongly tapered towards the head. The flow was forced by changing the rotation rate of the tank. The flow was observed using neutrally buoyant particles with the position of the particles noted at intervals and velocities calculated from position differences. Other than the initial density distribution (determined by the filling parameters) the density distribution was unknown so that all parameters were estimated from the measured velocity field. Particle depth was estimated in two ways. First the particles were illuminated by colored light using different colors above and below the shelf break depth. A more precise measure of the particle depth was obtained from a numerical model (S-Coordinate Rutgers University Model Version 3.1 (SCRUM) [Hedström, 1997]) configured to accurately reproduce the laboratory experiment.

[72] A second, similar but not identical canyon (Lab-Mirshak), was used in the same shelf/slope topography to

estimate the net effect of a canyon on spin-down [Mirshak and Allen, 2005]. The change in spin-down can be written as an extra drag caused by the canyon and assuming geostrophic flux one can estimate an on-shore flux through the canyon of

$$\Psi_o = \frac{F_D}{\rho f L} \quad (30)$$

where F_D is the drag force [Mirshak and Allen, 2005]. Results from these experiments will be used to verify the flux scaling.

[73] Carson canyon is a wide canyon (34 km) of moderate length (16 km) on the east coast of Newfoundland. Typical currents are downwelling favorable but in June 1981 the effects of a current reversal were documented by three current meters moored over the canyon [Kinsella *et al.*, 1987].

[74] A detailed CTD survey of a canyon off Tidra, Northwest Africa shows the effect of strong upwelling flows [Shaffer, 1976]. Tidra is a small canyon (width 10 km, length 5 km) with a sharp upstream corner ($\mathcal{R} = 2.7 \text{ km}$) at low latitude (20°N) so moderate flows (0.15 m s^{-1}) lead to high Rossby numbers.

[75] A laboratory study of impulsively started flow over a rotating was performed at the Arizona State University rotating table facility [Pérenne *et al.*, 2001]. Their canyon is wider and shorter than the Lab-Allen canyon used by Allen *et al.* [2003]. It is also less tapered with width at half-length almost 50% of the width at the shelf break. Velocity data was collected at three depths: above, at and below rim depth. This canyon will be referred to as “Pérenne-Lab”.

[76] Redondo submarine canyon is a narrow canyon with steeply sloping sides ($\approx 2 \text{ km}$ wide by 500 m deep) that projects into the Santa Monica Bay shelf (Figure 9). It extends to within 2 km of the coast. The flow is predominantly equatorward over the canyon in the upwelling season [Hickey *et al.*, 2003].

3.2. Comparisons of Scaling to Observations

3.2.1. Upwelling Flux

[77] As the experiments of Mirshak and Allen [2005] provide the largest number of data points and thus provide the best estimate of the function \mathcal{F} , we will begin by comparing the observed upwelling flux to the scaling estimate. We fit the non-dimensional observed upwelling flux

$$\frac{\Phi_o}{UW_{sb}D_h} = \frac{F_D}{\rho f LUW_{sb}D_h} \quad (31)$$

to the non-dimensional scaled flux

$$\frac{\Phi}{UW_{sb}D_h} = \mathcal{F}^{3/2} R_L^{1/2} = \left(\frac{c_1 R_o}{c_2 + R_o} \right)^{3/2} R_L^{1/2} \quad (32)$$

As we have no direct estimates of \mathcal{F} , it is not possible to determine c_1 ; it always appears multiplied by an unknown constant (in this case the scale for the flux). Hence we will assume $c_1 = 1$ and absorb it into the coefficients for the parameters that can be estimated.

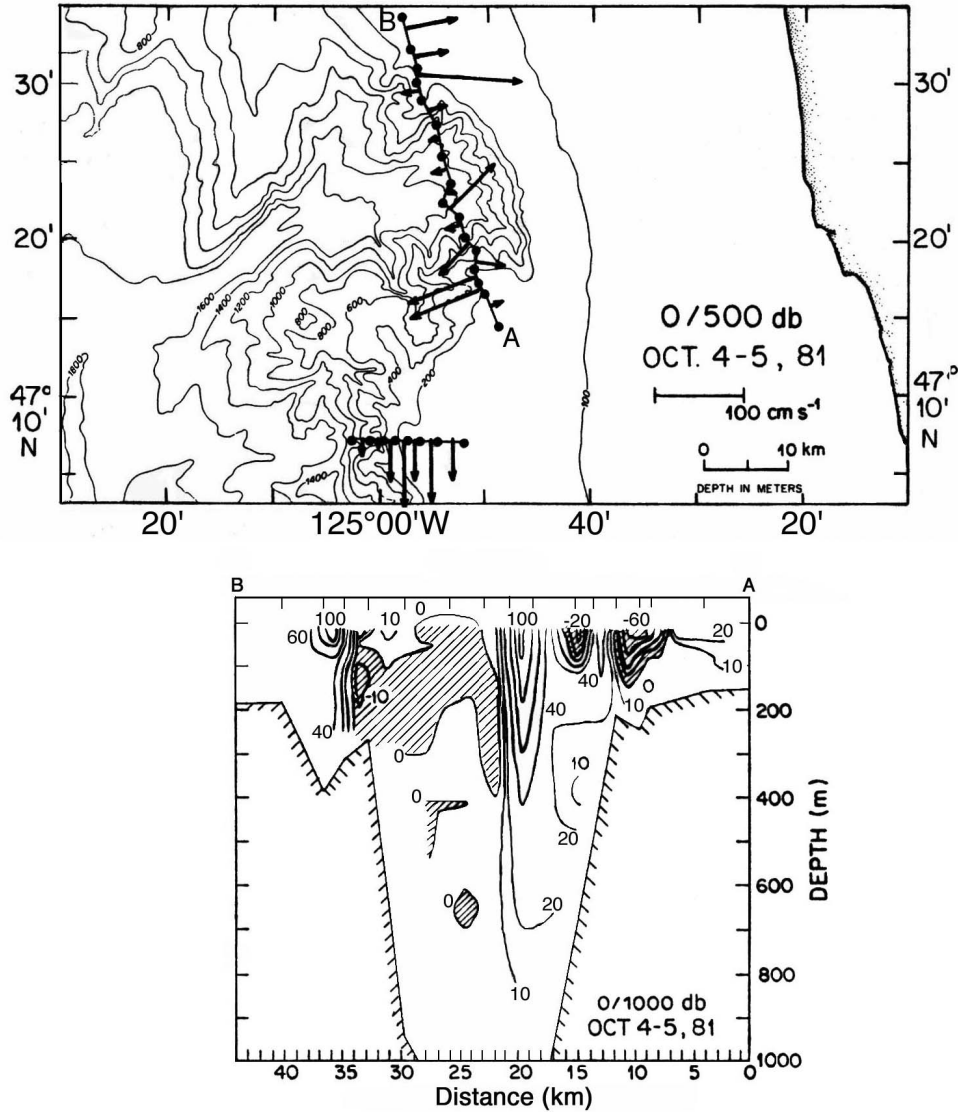


Figure 7. (top) Bathymetry of Quinault Canyon. Solid dots mark the location of CTD stations. Arrows give the geostrophic velocity (0/500 db) during an upwelling event. Data have been extrapolated into regions shallower than the reference level using the method of *Montgomery* [1941]. Geostrophic currents perpendicular to the CTD transects show the tendency for the flow to follow local isobaths. (bottom) Geostrophic velocity (0/1000 db) across Quinault Canyon during an upwelling event. Off shelf flow is shaded. The data are consistent with the presence of a rim eddy over the canyon and cyclonic vorticity deep in the canyon.

[78] Using the Levenberg-Marquandt algorithm for non-linear least-squares optimization, the observed non-dimensional flux (31) was fit to

$$c_3 c_2^{1.5} \left(\frac{R_o}{1 + R_o/c_2} \right)^{3/2} R_L^{1/2} \quad (33)$$

to give $c_2 = 0.9$ and $c_3 = 1.0$ (Figure 10) with an root mean square error of 26%. The value of c_2 is reasonably well constrained by the data; a value of 0.8 leads to a 33% error and a value of 0.95 leads to a 35% error.

3.2.2. Depth of Upwelling

[79] The depth of the deepest upwelling was estimated for each canyon in different ways, depending on the data available for each canyon.

3.2.2.1. Barkley Canyon

[80] To estimate the deepest depth of upwelling over Barkley Canyon in 1997 the densest water observed over the shelf (stations BCD2 (150 m depth) and BCC2 (172 m depth)) was compared to a CTD cast at the mouth of the canyon (BCC4 (772 m depth) (Figure 6)). In 1997, the densest water on the shelf, $26.64 \sigma_t$, was observed in the bottom boundary layer at BCC2 right at the head of the canyon. This water occurred at a depth of 226.5 m at the

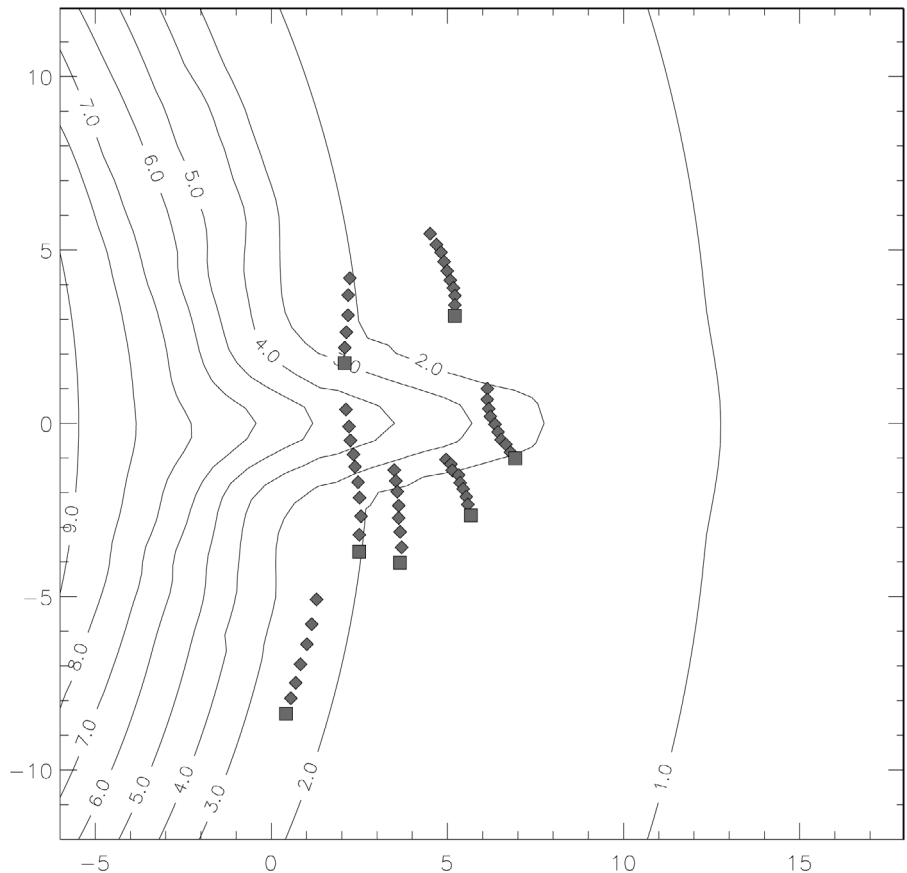


Figure 8. Bathymetry of the Lab-Allen canyon. All dimensions are in cm. The tank is cylindrical (radius 50 cm) with the coast and shelf running around the outside. The deep ocean is toward the center of the tank. The diamonds mark the sequential position (0.5 s apart) of tracers in the flow. The last position is marked by a square. All the tracers shown were at 1.5 cm to 1.6 cm depth (above the shelf break depth of 2.2 cm). The tracers show coastward flow over the downstream edge of the canyon consistent with upwelling. The tracers do not show any evidence of an eddy over the canyon.

canyon mouth and thus the deepest water upwelled onto the shelf came from deeper than 226.5 m. Similarly the deepest depth of upwelling was found from CTD sections for Astoria Canyon, Quinault Canyon, Barkley Canyon in 1998, Carson Canyon and the canyon off Tidra.

3.2.2.2. Astoria Canyon

[81] The Astoria Canyon calculation is based on a station at the mouth and a station at the head taken during an upwelling event in May 1983 (Figure 5).

3.2.2.3. Quinault Canyon

[82] The Quinault Canyon calculation was based on a survey in May, 1979 that fortuitously took place during an upwelling event.

3.2.2.4. Carson Canyon

[83] For Carson Canyon the depth of upwelling was estimated from the observed rise of the 1°C isotherm [Kinsella *et al.*, 1987, Figure 5].

3.2.2.5. Tidra Canyon

[84] For the canyon off Tidra it was estimated from the depth of the 26.7–26.8 σ_t averaged from stations 123, 124 and 140 versus mouth stations 132 and 125 [Shaffer, 1976, Figures 14, 17, and 20].

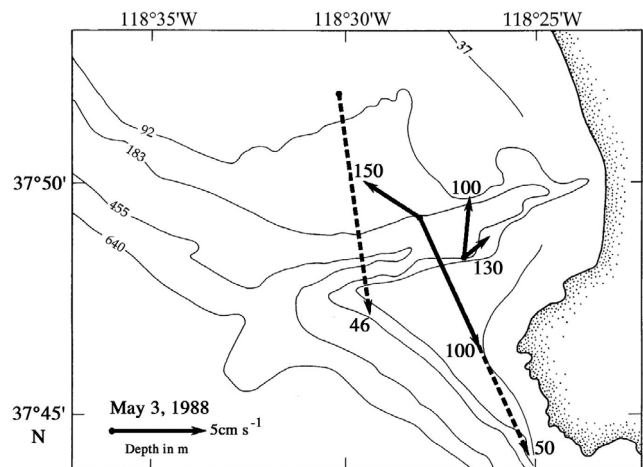


Figure 9. Bathymetry of Redondo Canyon. Solid and dotted arrows mark the currents below and above the rim of the canyon, respectively on May 3, 1988 during a strong upwelling event. Upper water column flow (46, 50, and 100 m) is directed across the canyon with little apparent influence by the canyon. A cyclonic circulation pattern occurs at and below rim depth (100 m; 130 and 150 m).

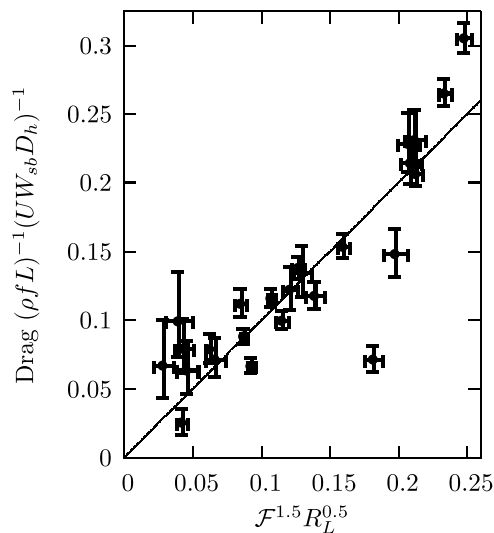


Figure 10. Flux through the canyon, observed versus the predicted scaling. The straight line (slope 1.0) is the best fit.

3.2.2.6. Lab-Allen Canyon

[85] For the Lab-Allen canyon [Allen *et al.*, 2003] the depth of upwelling was estimated from the depth of the deepest particle that was observed to upwell onto the shelf (1.9 cm). Extrapolating to the mouth of the canyon this particle would have originated from a depth of 2.0 cm.

3.2.2.7. Perenne-Lab Canyon

[86] For the Perenne-Lab canyon the depth of upwelling could not be determined beyond that it was less than 5 cm depth based on flow patterns at that depth [P erenne *et al.*, 2001, Figure 10a].

3.2.2.8. Redondo Canyon

[87] For Redondo Canyon the depth of deepest upwelling was derived from time series of temperature within and over the canyon. Specific upwelling events have been identified in previous research [Hickey *et al.*, 2003].

3.2.2.9. Results

[88] The observed deepest depth of upwelling is in reasonable agreement with predictions from the scaling analysis (Figure 11). The farthest departure from the line is Redondo Canyon where we expect different dynamics to hold due to its very close (≈ 2 km) approach to the coast. The linear fit of the observed to the predicted values (neglecting Redondo Canyon) gives

$$\frac{Z}{D_H} = 1.3(\mathcal{F}R_L)^{1/2} + 0.06 \quad (34)$$

with an average fractional error of 21%. The intercept is to be expected; even in the absence of a canyon, upwelling is occurring along the coast and this effect is not removed from the observations.

[89] The value measured from particle tracking (Lab-Allen Canyon) appears to be lower than the values measured from CTD profiles. The particle tracking method provides a lower limit as the whole water column is not sampled. The upwelling depth estimated from the current meter array at Redondo Canyon is higher than values for the other canyons. Water from 80 m is upwelled to 40 m in Redondo Canyon

consistent with the stronger upwelling expected in canyons which closely approach the coast [Allen, 2000].

3.2.3. Deep Vorticity

[90] Depending on what data was available for each canyon, deep vorticity within the canyons was estimated either from current meter records or by estimating stretching from density records.

3.2.3.1. Barkley Canyon

[91] The deep vorticity over Barkley Canyon in 1997 was estimated from CTD profiles at station BCC4 at the mouth of the canyon and at station BCC3 (630 m depth) in the centre of the canyon. The stretching was calculated for isopycnals $0.1 \sigma_t$ apart and averaged over the stretching region (215 m to 345 m). For 1998, the vorticity was based on the average of two stations in the canyon versus the average of a station upstream and downstream of the canyon.

3.2.3.2. Astoria Canyon

[92] For Astoria Canyon, deep stretching vorticity was estimated using upstream hydrographic data compared to in-canyon data to estimate changes in layer depth (Figure 12). Calculation of relative vorticity using the shear between current meters at similar depths gave a much smaller value of $0.2f$ rather than about $1.0f$. However, these current meters were at 230 m and thus perhaps were too shallow to sample the strongest stretching seen at 300 m depth.

3.2.3.3. Quinault Canyon

[93] On the other hand for Quinault Canyon, deep vorticity was estimated using along-canyon geostrophic flow on the two sides of the canyon during an upwelling event in May 1979 as well as the data shown in Figure 7 from an upwelling event in October 1981 [Hickey, 1989].

3.2.3.4. Lab-Allen Canyon

[94] For the Lab-Allen Canyon, the vorticity deep in the canyon was estimated from the shear between two deep particles, one on each side of the canyon.

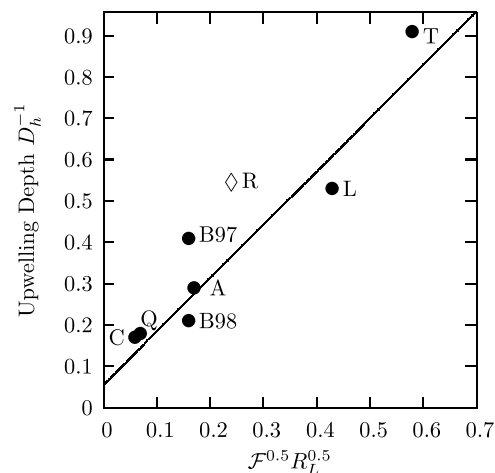


Figure 11. Depth of upwelling, observed versus the predicted scaling. The values are labeled: A-Astoria, B-Barkley (data from years 1997 and 1998), C-Carson, L-Lab-Allen, R-Redondo, Q-Quinault, and T-Tidra Canyon. Note the stronger upwelling observed in Redondo Canyon which closely approaches the coast and thus has different dynamics. The straight line (slope 1.3) is the best fit for the other canyons.

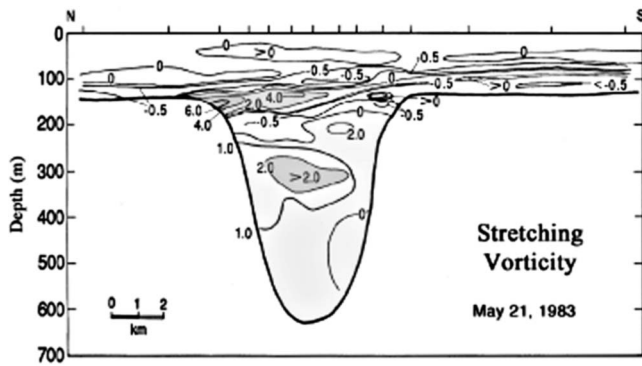


Figure 12. Stretching vorticity across Line 1 over Astoria Canyon (Figure 5) relative to a station upstream. Units are f . Shading marks cyclonic vorticity. Note the strong cyclonic vorticity deep in the canyon. Even stronger cyclonic vorticity is seen at rim depth in the vicinity of the observed rim depth eddy. From Hickey [1997].

3.2.3.5. Perenne-Lab Canyon

[95] For the Perenne-Lab canyon it was estimated from flow patterns at 5 cm depth [P erenne *et al.*, 2001, Figure 10].

3.2.3.6. Redondo Canyon

[96] For Redondo Canyon the deep vorticity was estimated from current meters at 130 and 150 m on opposite sides of the canyon (Figure 9).

3.2.3.7. Results

[97] The estimated deep vorticity shows a linear relationship with the observed deep vorticity for the four canyons excluding Redondo Canyon (Figure 13). The linear fit of the observed to the predicted values (neglecting Redondo Canyon) gives

$$S = 2.5(\mathcal{F}R_L)^{1/2} \frac{L}{W_{sb}} + 0.3 \tag{35}$$

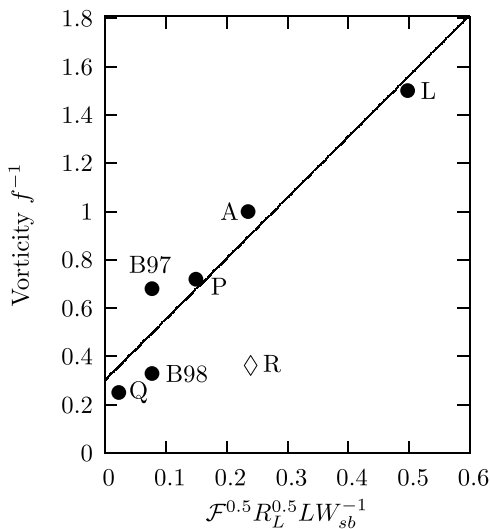


Figure 13. Deep vorticity, observed versus the predicted scaling. Labeling as in Figure 11. Note that the weakest vorticity is observed in Redondo Canyon illustrating the different dynamics over this canyon. The straight line (slope 2.5) is the best fit for the other canyons.

with an average error of 16%. The intercept is to be expected; even in the absence of a canyon, upwelling and thus stretching is occurring along the coast and this effect is not removed from the observations. Redondo Canyon has the weakest deep vorticity, again consistent with its distinctly different dynamics.

3.2.4. Eddy Presence

3.2.4.1. Barkley Canyon

[98] In 1997, the presence of a rim eddy over Barkley Canyon at 100 to 150 m depth is apparent in the currents derived from a diagnostic model [Allen *et al.*, 2001]. The eddy has a radius of 5 km and peak velocities of 30 cm s^{-1} with a vorticity of $0.3 f$ (Figure 6). The eddy was observed in 1998 using current meter observations. Average currents for Jul 25 show flow generally southward over the canyon at 150 m depth but the four current meters (Figure 6) clearly show a cyclonic eddy at 250 m depth.

3.2.4.2. Astoria Canyon

[99] For Astoria canyon, the presence of a rim eddy during upwelling was deduced from available current meter data near the rim (Figure 5).

3.2.4.3. Quinault Canyon

[100] Over Quinault canyon, the presence of a rim eddy was deduced from geostrophic velocities across the canyon during an upwelling event in October 1981 (Figure 7).

3.2.4.4. Carson Canyon

[101] An eddy is evident around Carson canyon from current meter observations [Kinsella *et al.*, 1987, Figure 8].

3.2.4.5. Tidra Canyon

[102] A 100-m deep drifter over the canyon off Tidra shows a rim depth eddy [Shaffer, 1976, Figure 44].

3.2.4.6. Lab-Allen Canyon

[103] The particle trajectories over the Lab-Allen Canyon clearly show that there is no rim-level eddy (Figure 8).

3.2.4.7. Perenne-Lab Canyon

[104] However, the broader Perenne-Lab canyon does have an eddy [P erenne *et al.*, 2001, Figure 7].

3.2.4.8. Redondo Canyon

[105] The presence of a rim eddy over Redondo Canyon was deduced from moored array data on two sides of the canyon (Figure 9).

3.2.4.9. Results

[106] The value of the eddy number for all 8 canyons is given in Table 3. All real canyons and the Perenne-Lab canyon had a rim depth eddy whereas the Lab-Allen canyon did not. Redondo Canyon, which closely approaches the coast, appears to fit the theory though this is probably fortuitous. The observations imply that the critical value of the

Table 3. Eddy Likelihood From Scaling Versus the Observation of the Presence or Absence of a Rim Depth Eddy^a

Canyon	E	Rim Eddy
Astoria	1.5	yes
Quinault	1.4	yes
Perenne	1.2	yes
Barkley '98	1.0	yes
Tidra	0.93	yes
Barkley '97	0.92	yes
Carson	0.92	yes
Redondo	0.76	yes
Lab-Allen	0.33	no

^aHere E is eddy likelihood from scaling.

Table 4. A Synopsis of the Simplified Scaling for Four Significant Components of the Upwelling Process for Small R_o^a

Feature	Symbol	Scaling	Effects						
			U	N	f	L	\mathcal{R}	W_{sb}	W
Depth of upwelling	Z	$1.4 \frac{U}{N} \left(\frac{L}{\mathcal{R}}\right)^{1/2}$	↑	↓	-	↑	↓	-	-
Upwelling flux	Φ	$1.2 \frac{U^3 W_{sb} L^{1/2}}{N f \mathcal{R}^{3/2}}$	↑↑	↓	↓	↑	↓	↑	-
Deep vorticity	Sf	$2.6 \frac{UL^{1/2}}{W_{sb} \mathcal{R}^{1/2}}$	↑	-	-	↑	↓	↓	-
Eddy presence	E	$1.0 \frac{fWL^{1/2}}{NH_s \mathcal{R}^{1/2}}$	-	↓	↑	↑	↓	-	↑

^aUpward/downward pointing arrows imply the component increases/decreases with the parameter. Strength of variation increases from ↑ to ↑↑ to ↓ to ↓↓.

eddy number for the presence of an eddy is greater than 0.33 and less than 0.92. So an eddy will be present if $E \geq 0.9$.

[107] The parameter E is primarily determined by the inverse of the Burger number fW/NH_s . Laboratory experiments have often been configured to match a field Burger Number based on the length of the canyon or the shelf break width. As laboratory canyons are often strongly tapered, the appropriate Burger number B_u is thus too high and rim depth eddies are not generated. The Pérenne experiments are an exception, with a much less tapered canyon and a small Burger number [Pérenne *et al.*, 2001].

4. Discussion

[108] The dynamics of upwelling over submarine canyons are nonlinear and complex. Even small topographic variations can cause significant changes in velocity and density fields [Klinck *et al.*, 1999]. However the study presented here shows that the basic response of the stratified fluid within and above the canyon can be estimated from bulk geometric parameters. The scaling analysis was performed assuming near-steady advection-driven upwelling driven by the flow that is nearly uniform over the length of the canyon. The canyon is assumed not to closely approach a coast (the distance between the coast and the head of the canyon is greater than $0.5(UX/f)^{1/2}$ where X is the distance from the coast to the H_h isobath away from the canyon [Allen, 2000]). These assumptions eliminate the initial transient upwelling which occurs as an equatorward wind event starts, and also eliminate from consideration canyons such as Juan de Fuca Canyon (approaches coast), Monterey Canyon (regional flow is non-uniform) and Redondo Canyon (approaches coast). However the analysis is applicable to the majority of canyons along the shelf break of the West Coast of Canada and the United States and in other regions where upwelling occurs and where and/or when the undercurrent is not present or lies below shelf break depth.

[109] As we proceeded through the scaling analysis we made further simplifying assumptions (Section 2.5). These restrict the analysis to steep-sided, narrow, deep canyons cutting into sloped continental shelves that are not overly deep. The canyons must be steep enough that the Ekman layers arrest within a day [Brink and Lentz, 2010]. We have assumed the canyons are less than two Rossby radii wide

and deep enough that the upwelling stream does not reach the bottom. The continental shelf is assumed to have a slope and be shallow enough that the shelf Burger Number based on the length of the canyon is less than 2. All these assumptions are met by the real canyons presented here.

[110] The scaling analysis was tested for four measurable quantities against observations collected in the field and data collected from three laboratory canyons. The reasonable agreement between the observed values and the predicted values gives us confidence in the scaling analysis. A least squares fit was used to set scalar coefficients for the scaled parameters.

[111] While deriving the scaling analysis, an estimate for the size of the scalar coefficients was made. The coefficient for the deepest depth of upwelling, 1.3, is close to 1, as expected; the coefficient for the vorticity, 2.5, is close to 2, as expected; the critical number for the presence of an eddy, between 0.33 and 0.92, is close to 1/2 and the coefficient c_2 in \mathcal{F} 0.9 is close to 1 as expected. The only deviation between our initial expectations and the observations occurs with the coefficient for the upwelling flux, that we expected to close to 1/4 and is actually 1. The difference is partially due to the difference in what was estimated and what was measured. The estimate was for the upwelling stream alone. However, the measurement will include all water turned through the canyon (including the rim depth stream) to give a total onshore flux. The fit here implies that the rim depth stream has 3 times the volume of the upwelling stream. Note that this does not include the extra onshore flux that occurs if the continental shelf is flat, because the Lab-Mirshak canyon shelf is sloped.

[112] For most real-world canyons, the Rossby number R_o is small (<0.5) and \mathcal{F} [defined in (13)] can be approximated by $1.1R_o$. This approximation allows simplification of the scaling (Table 4). In particular, the depth of upwelling can be expressed as $Z = 1.4(U/N) \times (L/\mathcal{R})^{1/2}$. Thus the depth of upwelling is linearly proportional to the strength of the flow across the canyon and inversely proportional to the strength of the stratification. Longer canyons and canyons with sharp inflow regions will have stronger upwelling.

[113] Making the same approximation for upwelling flux gives

$$\Phi = 1.2 \left(\frac{U^3 W_{sb} L^{1/2}}{N f \mathcal{R}^{3/2}} \right) \quad (36)$$

Thus upwelling flux is proportional to the cube of the strength of the flow across the canyon. The flux is stronger for wider or longer canyons and for canyons with sharp inflow regions and the flux is inversely proportional to the strength of the stratification. This steady upwelling flux for Astoria Canyon is equivalent to a wind-driven Ekman mass flux due to a 16 m s^{-1} wind or about twice the flux that would be associated with the actual observed peak Bakun wind over the canyon during the 1983 measurements.

[114] Similarly, the vorticity in the deep water can be expressed as $Sf = 2.6U\mathcal{R}^{-1/2} L^{1/2} W_{sb}^{-1}$. Thus the vorticity deep in the canyon increases with the strength of flow across the canyon and is independent of the stratification. Vorticity is stronger for longer canyons and weaker for wider canyons or for canyons with smoother inflow regions.

[115] The condition for an eddy at rim depth is E large and for small Rossby number $E \approx fWL^{1/2}/(NH_s\mathcal{R}^{1/2})$. The likelihood of an eddy increases with the ability of the fluid column to generate vorticity by stretching fW/NH_s and with the ratio of the canyon length to radius of curvature. All the real canyons studied here had eddy numbers greater than 0.7 and rim depth eddies were observed over each of these canyons. The generic canyons of some previous modeling studies [e.g., *Allen et al.*, 2003] are generally too triangular (narrow near the head $W \ll NH_s/f$) to have rim eddies. Realistic canyons taper much less towards the head than has often been assumed in modeling studies. The canyon used in the *Pérenne et al.* [2001] study has a more realistic horizontal shape.

[116] One of the most important geometric parameters is the shape of the shelf break upstream of the mouth of the canyon. The radius of curvature of this region, \mathcal{R} , determines the tendency of the flow to cross the canyon bathymetry. Many canyons (Astoria, Figure 5; Barkley, Figure 6) appear to have fans in this area which increase the radius of curvature. These fans may be due to winter sediment fluxes from the canyon being transported poleward by the winter poleward currents. These fans greatly increase \mathcal{R} and thus decrease upwelling within the canyon. Recent results for a buoyancy current traveling over a canyon found a similar importance of the upstream radius of curvature as to whether the current crossed the canyon (separated) or flowed into the canyon [*Sutherland and Cenedese*, 2009].

[117] The upwelling flux data used in this paper were measured in a laboratory study by *Mirshak and Allen* [2005]. Those authors used an empirical scaling to determine the dependence of the flux on powers of N , U and f : flux varied as $U^2(U/f)^n N^{-1}$, where $n = 0.66 \pm 0.35$. Length scales were not varied in their study. Here we find the same relationship with respect to N and between U and f . However, our relationship for flux as a function of Ro ($\approx U/f$) is not a simple power relationship because of the shape of the \mathcal{F} function (13). When plotted over the measured range of Ro and compared to the power law relationship including its error the new relationship falls within the bounds of the *Mirshak and Allen* [2005] relationship (not shown). Thus, over the range of Ro used (0.2–1.0) the two relationships are not significantly different. However, the new dynamically based relationship predicts more moderate upwelling at high Rossby number: this result is more realistic than the power law relationship of *Mirshak and Allen* [2005] which fails as Ro goes to infinity.

[118] *Mirshak and Allen* [2005] did not vary the shape of the canyon and thus the dependence on canyon length scales was assumed and not determined. They extrapolated their laboratory results to Astoria Canyon based on the similarity between the shapes of the canyons. However, the ratio between the radius of curvature and the length of Astoria Canyon is twice as large in the laboratory canyon. This led them to underestimate of the flux through Astoria Canyon compared to the more thorough analysis given here.

[119] Our parameterizations for other canyon variables such as depth of upwelling and vorticity provide estimates consistent with real world observations, suggesting that our general approach is correct. We have no field observations for flux; however, our results can be compared to previous scaling analyses. For oscillatory flow over a canyon:

dependencies for the net flux through the canyon on stratification, flow speed and Coriolis parameter are similar to ours; the flux increases with increasing flow speed, whereas increasing stratification and Coriolis parameter decrease the flux [*Boyer et al.*, 2004; *Haidvogel*, 2005]. Length-scale dependence has not been analyzed for oscillatory flow [*Boyer et al.*, 2006]. However a scaling analysis for steady flow (similar to our analysis) that was based purely on numerical results [*Kämpf*, 2007] differs substantially from our results. Dependence on stratification is consistent with our results. However, the *Kämpf* [2007] dependence on the Coriolis parameter is in the opposite direction from ours: ours decreases upwelling flux as f increases, whereas his increases the flux. Applying the final formula by *Kämpf* [2007] to laboratory canyons gives erroneously large results, implying that its dependence on f cannot be extrapolated to the high values found in the laboratory. The dependence on incoming flow is more similar in the two analyses: however, our dependence is stronger, being proportional to the cube of the incoming flow rather than the square. The length-scale dependence of the flux for the *Kämpf* study is simply the depth of the canyon whereas ours is its length and width. The canyon depth does not appear in our analysis because we are assuming much deeper canyons. Our shallowest canyon, Barkley Canyon, has a shelf break to center depth of over 350 m. *Kämpf* [2007] is considering canyons from 45–230 m deep. Another type of comparison is to apply the estimates of *Kämpf* [2007] and our estimates to the real canyons for which there is data. Comparing the values of flux through the canyons, our fluxes are substantially (1.6 to 29 times) smaller than his.

[120] The difference between the estimates appears to be the slope of the continental shelf. The central case canyon from *Kämpf* [2007] is within the parameter range studied here for the other restrictions (Section 2.5). It does indeed have uniform moderate flow and uniform stratification near rim depth, and it is narrow and regular. It is deep enough that the upwelling flux should be unaffected by the canyon depth (which would not be true for the shallower canyons considered by *Kämpf* [2007]). The numerical canyon is not as steep as the canyons considered here and given the same drag coefficient as used by *Brink and Lentz* [2010] would not have arrested bottom boundary layers for the first 3.5–3.9 days. However, the linear friction coefficient used ($7 \times 10^{-4} \text{ m s}^{-1}$) in the numerical model gives a higher drag which should lead to arrested boundary layers within a day. Our conjecture is that the crucial difference between the numerical canyons of *Kämpf* [2007] and the canyons considered here is that *Kämpf* [2007] uses a flat continental shelf. Thus in addition to the flux estimated here, the flux over his canyons includes a branch of the incoming flow that follows the canyon rim to the head of the canyon and is not turned back to the shelf break by the shelf-topographic slope. Note that the final formula presented by *Kämpf* [2007] cannot be extrapolated to laboratory settings.

[121] Few submarine canyons have been studied with the detail of Astoria or Barkley Canyon. The scaling presented here for upwelling over coastal submarine canyons allows estimation of the effects of upwelling over the many unstudied canyons with minimal measurements. Besides detailed bathymetry (to estimate the geometric parameters \mathcal{R} , L , W_{sb} and W), a local CTD cast (to estimate N near rim

depth) and local current meter data upstream of the canyon (to estimate the incoming, near shelf bottom velocity U during an upwelling event) are required to perform the suggested scaling. Given these parameters, the depth of upwelling in the canyon can be estimated to within 15 m, the deep vorticity can be estimated to within 15% and the presence or absence of a rim depth eddy can be determined. Based on the laboratory data, total upwelling flux can also be estimated.

[122] The scale analysis developed herein demonstrates the important point that in spite of very steep topography and variable spatial structures, some aspects of canyon dynamics in upwelling environments obey relatively robust and simple relationships. This information can be used to advantage in regions where detailed canyon data are lacking. In particular, one of the reasons canyons are of great interest is that they are known to enhance cross-shelf exchange of properties such as carbon and nutrients. The relationships presented here can be used to estimate such fluxes within a given region that includes canyons with a reasonable degree of certainty. In addition, we expect that the relationships for depth of upwelling, deep vorticity and eddy presence, which are strongly constrained by data from a number of canyons, will provide critical benchmarks for future modeling in canyon regions.

Notation

- a Rossby radius NH_s/f .
- B_c non-dimensional canyon depth $NH_c/(fL)$.
- B_s non-dimensional shelf break depth $NH_s/(fL)$.
- B_u Burger number $NH_s/(fW)$.
- D_H depth scale fL/N .
- D_w scale depth deep in the canyon $fW_{sb}/(2N)$.
- E eddy number fWZ/UH_s .
- Ek Ekman number $\nu/(fH_s^2)$.
- f Coriolis parameter.
- \mathcal{F} a function of R_o defined in (13).
- g gravitational acceleration.
- h fluid column length.
- H_c depth change across the canyon mouth
- H_h depth at the head of the canyon.
- H_s shelf break depth.
- \hat{k} vertical unit vector.
- ℓ unspecified horizontal length scale.
- L length of the canyon.
- M ND shelf-slope $(H_s - H_h)fL/(H_sU)$
- N Brunt-Väisälä frequency near rim depth.
- (r, θ) polar coordinates around the projected center of the upstream isobaths.
- R radius of curvature of streamlines (natural coordinates).
- \mathcal{R} radius of curvature of shelf break isobath upstream of canyon.
- p pressure.
- R_L Rossby number U/fL .
- R_o Rossby number $U/f\mathcal{R}$.
- R_w Rossby number U/fW_{sb} .
- (s, n) natural coordinates, s along flow, n across flow.
- S stretching deep in the canyon.
- T isopycnal tilt along the canyon.

$\vec{u} = (\vec{u}_h, w)$ flow velocity: horizontal and vertical components.

- U strength of velocity upstream of the canyon.
- U_D velocity scale deep in the canyon.
- U_* strength of upwelling stream.
- V strength of flow across the canyon at rim depth.
- W width of canyon at half-length.
- W_{sb} width of canyon at shelf break.
- u horizontal velocity in natural coordinates.
- (u_r, u_θ) polar, horizontal, velocity components.
- z vertical distance, positive upwards.
- Z vertical depth change of deepest isopycnal upwelled onto shelf.
- Γ strength of horizontal density perturbations.
- Φ flux of water upwelled onto shelf.
- ρ density.
- ρ_o constant reference density.
- ρ_* horizontally uniform, undisturbed density.
- ν viscosity or eddy viscosity
- Ω strength of vertical velocity.
- ζ vertical component of relative vorticity.

[123] **Acknowledgments.** This work was supported by National Science and Engineering Strategic and Discovery Grants to S. Allen and by grants to B. Hickey from the U.S. National Science Foundation (OCE-9618186, OCE-0234587, and OCE-0239089) and from the Center for Sponsored Coastal Ocean Research of the National Ocean and Atmospheric Administration (NA17OP2789). This is contribution 50, 25, and 324 of the RISE, ECOHAB PNW, and ECOHAB programs, respectively. The statements, findings, conclusions, and recommendations are those of the authors and do not necessarily reflect the views of the NSF, NOAA, or the Department of Commerce. The authors thank N. Banas, M. Dinniman, J. Klinck, R. Mirshak, and A. Waterhouse for comments on earlier versions of the manuscript and an anonymous referee whose insightful comments led to the analysis of the restrictions on the cases considered.

References

- Allen, S. E. (1996), Topographically generated, subinertial flows within a finite length canyon, *J. Phys. Oceanogr.*, *26*, 1608–1632.
- Allen, S. E. (2000), On subinertial flow in submarine canyons: Effect of geometry, *J. Geophys. Res.*, *105*, 1285–1297.
- Allen, S. E., and X. Durrieu de Madron (2009), A review of the role of submarine canyons in deep-ocean exchange with the shelf, *Ocean Sci.*, *5*, 607–620.
- Allen, S. E., C. Vindeirinho, R. E. Thomson, M. G. G. Foreman, and D. L. Mackas (2001), Physical and biological processes over a submarine canyon during an upwelling event, *Can. J. Fish. Aquat. Sci.*, *58*, 671–684.
- Allen, S. E., M. S. Dinniman, J. M. Klinck, D. D. Gorby, A. J. Hewett, and B. M. Hickey (2003), On vertical truncation errors in terrain following numerical models: Comparison to a laboratory model for upwelling over submarine canyons, *J. Geophys. Res.*, *108*(C1), 3003, doi:10.1029/2001JC000978.
- Boyer, D. L., D. B. Haidvogel, and N. Pérenne (2004), Laboratory-numerical model comparisons of canyon flows: A parameter study, *J. Phys. Oceanogr.*, *34*, 1588–1609.
- Boyer, D. L., J. Sommeria, A. S. Mitrovic, V. K. C. Pakala, S. A. Smirnov, and D. Etling (2006), Effects of boundary turbulence on canyon flows forced by periodic along-shelf currents, *J. Phys. Oceanogr.*, *36*, 813–826.
- Brink, K. H., and S. J. Lentz (2010), Buoyancy arrest and bottom Ekman transport. Part I: Steady flow, *J. Phys. Oceanogr.*, *40*, 621–635.
- Buckingham, E. (1914), On physically similar systems: Illustrations on the use of dimensional equations, *Phys. Rev.*, *4*, 345–376.
- Dawe, J. T., and S. E. Allen (2010), Solution convergence of flow over steep topography in a numerical model of canyon upwelling, *J. Geophys. Res.*, *115*, C05008, doi:10.1029/2009JC005597.
- Flexas, M. M., D. L. Boyer, M. Espino, J. Puigdefàbregas, A. Rubio, and J. B. Company (2008), Circulation over a submarine canyon in the NW Mediterranean, *J. Geophys. Res.*, *113*, C12002, doi:10.1029/2006JC003998.
- Freeland, H. J., and K. L. Denman (1982), A topographically controlled upwelling center off southern Vancouver Island, *J. Mar. Res.*, *40*, 1069–1093.

- Haidvogel, D. B. (2005), Cross-shelf exchange driven by oscillatory barotropic currents at an idealized coastal canyon, *J. Phys. Oceanogr.*, *35*, 1054–1067.
- Hedström, K. S. (1997), User's manual for an s-coordinate primitive equation ocean circulation model (SCRUM): Version 3.0, *Rep. 97-10*, Inst. of Mar. and Coastal Sci., Rutgers Univ., New Brunswick, N. J.
- Hickey, B. M. (1989), Patterns and processes of circulation over the Washington continental shelf and slope, in *Coastal Oceanography of Washington and Oregon, Elsevier Oceanogr. Ser.*, vol. 47, edited by M. R. Landry and B. M. Hickey, pp. 41–115, Elsevier Sci., Amsterdam.
- Hickey, B. M. (1995), Coastal submarine canyons, in *Topographic Effects in the Ocean*, edited by P. Muller and D. Henderson, pp. 95–110, Univ. of Hawaii at Mānoa, Honolulu.
- Hickey, B. M. (1997), The response of a steep-sided narrow canyon to strong wind forcing, *J. Phys. Oceanogr.*, *27*, 697–726.
- Hickey, B. M., and N. S. Banas (2008), Why is the northern end of the California current system so productive?, *Oceanography*, *21*, 90–107.
- Hickey, B. M., E. Baker, and N. Kachel (1986), Suspended particle movement in and around Quinault Submarine Canyon, *Mar. Geol.*, *71*, 35–83.
- Hickey, B. M., R. E. Thomson, H. Yih, and P. H. LeBlond (1991), Velocity and temperature fluctuations in a buoyancy-driven current off Vancouver Island, *J. Geophys. Res.*, *96*, 10,507–10,538.
- Hickey, B. M., E. Dobbins, and S. E. Allen (2003), Local and remote forcing of currents and temperature in the central Southern California Bight, *J. Geophys. Res.*, *108*(C3), 3081, doi:10.1029/2000JC000313.
- Holton, J. R. (1992), *An Introduction to Dynamic Meteorology*, 3rd ed., 511 pp., Academic, San Diego, Calif.
- Jaramillo, S. (2005), Numerical simulation of flow in a laboratory tank using a z-coordinate numerical model, M.S. thesis, Univ. of B. C., Vancouver, B. C., Canada.
- Kämpf, J. (2007), On the magnitude of upwelling fluxes in shelf-break canyons, *Cont. Shelf Res.*, *27*, 2211–2223.
- Kinsella, E. D., A. E. Hay, and W. W. Denner (1987), Wind and topographic effects on the Labrador current at Carson canyon, *J. Geophys. Res.*, *92*, 10,853–10,869.
- Klinck, J. M. (1988), The influence of a narrow transverse canyon on initially geostrophic flow, *J. Geophys. Res.*, *93*, 509–515.
- Klinck, J. M. (1989), Geostrophic adjustment over submarine canyons, *J. Geophys. Res.*, *94*, 6133–6144.
- Klinck, J. M. (1996), Circulation near submarine canyons: A modeling study, *J. Geophys. Res.*, *101*, 1211–1223.
- Klinck, J. M., B. M. Hickey, M. S. Dinniman, and S. E. Allen (1999), Model-data comparison of flow over realistic topography in a region with coastal submarine canyons, in *EOS Trans. AGU*, *80*(49), Ocean Sci. Meet. Suppl., OS22L.
- Krassovski, M. (2008), Investigation of the California Undercurrent off the west coast of Vancouver Island, M.S. thesis, Univ. of Victoria, Victoria, B. C., Canada.
- MacCready, P., and P. B. Rhines (1991), Buoyant inhibition of Ekman transport on a slope and its effect on stratified spin-up, *J. Fluid Mech.*, *223*, 631–661.
- Mackas, D. L., R. Kieser, M. Saunders, D. R. Yelland, R. M. Brown, and D. F. Moore (1997), Aggregation of euphysiids and Pacific Hake (*Merluccius productus*) along the outer continental shelf off Vancouver Island, *Can. J. Fish. Aquat. Sci.*, *54*, 2080–2096.
- Mirshak, R., and S. E. Allen (2005), Spin-up and the effects of a submarine canyon: Applications to upwelling in Astoria Canyon, *J. Geophys. Res.*, *110*, C02013, doi:10.1029/2004JC002578.
- Montgomery, R. B. (1941), Transport of the Florida Current off Havana, *J. Mar. Res.*, *4*, 198–219.
- Pérenne, N., J. W. Lavelle, D. C. I. Smith, and D. L. Boyer (2001), Impulsively started flow in a submarine canyon: Comparison of results from laboratory and numerical models, *J. Atmos. Oceanic Technol.*, *18*, 1698–1718.
- Pereyra, W. T., W. G. Pearcy, and F. E. J. Carvey (1969), *Sebastes flavidus*, a shelf rockfish feeding on mesopelagic fauna, with consideration of the ecological implications, *J. Fish. Res. Board Can.*, *26*, 2211–2215.
- Shaffer, G. (1976), A mesoscale study of coastal upwelling variability off NW-Africa, *Meteor. Forschungsergeb. Reihe A*, *17*, 21–72.
- She, J., and J. M. Klinck (2000), Flow near submarine canyons driven by constant winds, *J. Geophys. Res.*, *105*, 28,671–28,694.
- Skliris, N., A. Goffart, J. H. Hecq, and S. Djenidi (2001), Shelf-slope exchanges associated with a steep submarine canyon off Calvi (Corsica, NW Mediterranean Sea), *J. Geophys. Res.*, *106*, 19,883–19,901.
- Sutherland, D. A., and C. Cenedese (2009), Laboratory experiments on the interactions of a buoyant coastal current with a canyon: Application to the East Greenland Current, *J. Phys. Oceanogr.*, *39*, 1258–1271.
- Vindeirinho, C. (1998), Water properties, currents and zooplankton distribution over a submarine canyon under upwelling-favorable conditions, M.S. thesis, Univ. of B. C., Vancouver, B. C., Canada.
- Waterhouse, A. F., S. E. Allen, and A. W. Bowie (2009), Upwelling flow dynamics in long canyons at low Rossby number, *J. Geophys. Res.*, *114*, C05004, doi:10.1029/2008JC004956.

S. E. Allen, Department of Earth and Ocean Sciences, University of British Columbia, 6339 Stores Rd., Vancouver, BC V6T 1Z4, Canada. (sallen@eos.ubc.ca)

B. M. Hickey, School of Oceanography, University of Washington, Box 357940, Seattle, WA 98105, USA. (bhickey@u.washington.edu)